การพัฒนาระบบถ่ายภาพด้วยนิวตรอนเร็วโดยใช้เครื่องกำเนิดนิวตรอนแบบพกพา

นางสาวเชีย เจีย ยี

วิทยานิพนธ์นี้เป็นส่วนหนึ่งของการศึกษาตามหลักสูตรปริญญาวิทยาศาสตรมหาบัณฑิต

สาขาวิชาเทคโนโลยีนิวเคลียร์ ภาควิชาวิศวกรรมนิวเคลียร์

คณะวิศวกรรมศาสตร์ จุฬาลงกรณ์มหาวิทยาลัย

ปีการศึกษา 2558

DEVELOPMENT ON FAST NEUTRON RADIOGRAPHY SYSTEM BY USING PORTABLE

NEUTRON GENERATOR

Miss Chia Jia Yi

A Thesis Submitted in Partial Fulfillment of the Requirements

for the Degree of Master of Science Program in Nuclear Technology

Department of Nuclear Engineering

Faculty of Engineering

Chulalongkorn University

Academic Year 2015

Thesis Title	DEVELOPMENT ON FAST NEUTRON RADIOGRAPHY SYSTEM BY USING PORTABLE NEUTRON GENERATOR
By	Miss Chia Jia Yi
Field of Study	Nuclear Technology
Thesis Advisor	Associate Professor Dr. Sunchai Nilsuwankosit

Accepted by the Faculty of Engineering, Chulalongkorn University in Partial Fulfillment of the Requirements for the Master's Degree

....Dean of the Faculty of Engineering

(Professor Dr. Bundhit Eua-arporn)

THESIS COMMITTEE

....Chairman

(Associate Professor Nares Chankow)

....Thesis Advisor

(Associate Professor Dr. Sunchai Nilsuwankosit)

....Examiner

(Associate Professor Somyot Srisatit)

....External Examiner

(Professor Dr. AMRAN BIN AB. MAJID)

เชีย เจีย ยี : การพัฒนาระบบถ่ายภาพด้วยนิวตรอนเร็วโดยใช้เครื่องกำเนิดนิวตรอนแบบ พกพา (DEVELOPMENT ON FAST NEUTRON RADIOGRAPHY SYSTEM BY USING PORTABLE NEUTRON GENERATOR) อ.ที่ปรึกษาวิทยานิพนธ์หลัก: รศ.สัญชัย นิล สุวรรณโฆษิต, 73 หน้า.

วัตถุระเบิดและวัตถุอันตรายที่ซุกซ่อนส่วนใหญ่นั้นมีลักษณะทางกายภาพไม่แตกต่างจาก วัตถุธรรมดาที่ประกอบด้วยธาตุหลัก H, C, N และ O เมื่อเปรียบเทียบกับระบบตรวจสอบทั่วไปที่ใช้ รังสีเอกซ์ การใช้ระบบถ่ายภาพด้วยนิวตรอนซึ่งตอบสนองได้ดีกว่ากับธาตุมวลเบาจึงมีความเหมาะสม กว่าในการตรวจสอบวัตถุที่ประกอบจากธาตุดังระบุข้างต้น เนื่องจากค่าใช้จ่ายที่แพงกว่าในการ ก่อสร้าง ความปลอดภัยในการใช้งาน รวมถึงสภาพที่ไม่สามารถเคลื่อนย้ายของแกนปฏิกรณ์วิจัย การ ถ่ายภาพโดยใช้นิวตรอนจากเครื่องกำเนิดนิวตรอนแบบพกพาจึงเป็นทางเลือกที่พิจารณาเนื่องจาก นิวตรอนที่ผลิตได้จากเครื่องกำเนิดนิวตรอนแบบพกพานั้นส่วนใหญ่เป็นนิวตรอนพลังงานสูง ระบบที่ พิจารณาจึงต้องเน้นการใช้นิวตรอนพลังงานสูงในการถ่ายภาพ ในการลดผลกระทบจากรังสีเอกซ์ที่ เกิดขึ้นพร้อม ๆ กันจากเครื่องกำเนิดนิวตรอนนั้นจะใช้ฉากรับรังสีหลังวัสดุที่ต้องการถ่ายภาพซึ่ง ประกอบขึ้นจากวัสดุขวางกั้นนิวตรอนที่ประกบหน้าหลังด้วยแผ่นสร้างภาพจากรังสี ในการนี้แผ่นอค ริลิกซึ่งมีความสามารถในการลดทอนนิวตรอนพลังงานสูงแต่ยังคงโปร่งใสกับรังสีเอกซ์จึงถูกใช้เป็นวัสดุ ขวางกั้นนิวตรอน ภาพที่ได้จากแผ่นร้างภาพจะถูกดำเนินการด้วยกะบวนการ XOR เพื่อแยกเอาข้อมูล เฉพาะจากการฉายด้วยนิวตรอน ภาพที่ได้จากแผ่นสร้างภาพทั้งสองแสดงให้เห็นอย่างชัดเจนว่ารังสี เอกซ์มีผลอย่างมากกับภาพที่ได้ และกระบวนการ XOR สามารถช่วยขยายผลจากนิวตรอนให้ชัดเจน ขึ้นได้ ผลที่ได้นี้ยืนยันว่าการถ่ายภาพวัตถุซึ่งประกอบขึ้นจาก H, C, N และ O นั้นสามารถกระทำได้ โดยใช้นิวตรอนพลังงานสูง ซึ่งกระบวนการนี้จะเป็นประโยชน์อย่างมากในการตรวจจับวัตถุระเบิดและ วัตถุอันตรายซึ่งประกอบด้วยธาตุดังกล่าว

ภาควิชา   วิศวกรรมนิวเคลียร์   ลายมือชื่อนิสิต ....

สาขาวิชา   เทคโนโลยีนิวเคลียร์   ลายมือชื่อ อ.ที่ปรึกษาหลัก ....

ปีการศึกษา 2558

5670565721 : MAJOR NUCLEAR TECHNOLOGY

KEYWORDS: FAST NEUTRON RADIOGRAPHY, NEUTRON GENENRATOR, ORGANIC MATERIAL DETECTION, BOOLEAN OPERATION ON GREY IMAGES

CHIA JIA YI: DEVELOPMENT ON FAST NEUTRON RADIOGRAPHY SYSTEM BY USING PORTABLE NEUTRON GENERATOR. ADVISOR: ASSOC. PROF. DR. SUNCHAI NILSUWANKOSIT, 73 pp.

Most of the concealed explosives and hazardous materials share the similar physical characteristics with the benign materials and are consisted of almost exclusively the elements H, C, N, and O. In comparison to the conventional X-ray inspection system, the neutron radiography is more sensitive with the light elements and, therefore, is more suitable for detecting the materials composed of such elements. Due to the high installation cost, the safety concern and the immobility of the research reactors, the neutron radiography system based on a portable neutron generator is proposed. Since the neutrons generated from a portable neutron generator are mostly the fast neutrons, the system is emphasized on using the fast neutrons for the purpose of conducting the radiography. In order to suppress the influence of X-ray produced by the neutron generator, a combination of a neutron shielding material sandwiched between two identical imaging plates is used as a screen behind the exposed material. An acrylic plate was used as the neutron shielding material as it can attenuate the fast neutrons but remains essentially transparent to the X-ray. A binary XOR operation is then applied on the images obtained by the two imaging plates in order to extract the information regarding the neutron exposure. The raw images obtained confirm that the X-ray really has a large effect and that XOR operation can help enhance the effect of the neutrons. The results also confirm that the fast neutron radiography of the concealed materials composed of H, C, N and O is possible. This can then be useful for detecting the concealed explosive materials composed of such elements.

Department:	Nuclear Engineering	Student's Signature ....
Field of Study:	Nuclear Technology	Advisor's Signature ....
Academic Year:	2015	

ACKNOWLEDGEMENTS

CONTENTS

LIST OF TABLES

จุฬาลงกรณ์มหาวิทยาลัย
CHULALONGKORN UNIVERSITY

LIST OF FIGURES

CHAPTER 1

INTRODUCTION

In this chapter, the background and rational of this study was discussed. The neutron radiography technique also was summarized. The discussion then was followed by the problem statement, the objective and the scopes of this study. The last part of this chapter discussed about the historical development and the research related to the fast neutron radiography.

1.1 Background

The terrorist events and the increase in the trade of illicit drugs remained the serious threats to the community in 21st century. In 2013, there was a total of 11,984 terrorist attacks occurred worldwide and around 62% (7,390 cases) of them involved the using of the explosives (bombings) [1]. The explosives were the popular terrorist weapons because of its potential for the high casualties and the severe property damage. On the other hand, the illicit drug use had a profoundly negative effect on a person's health, life quality and might lead to the premature death in some cases such as the overdose. In this era of globalization, the materials, technology and information transfer worldwide had facilitated the international terrorism and the trafficking of illicit drugs. Therefore, it is necessary to seek a technique that could detect these contrabands effectively.

Most of the hazardous materials had the similar physical appearance with most of the benign materials and consisted almost exclusively of the elements H, C, N, and O. Figure 1.1 showed the atomic fractions of the elements H, C, N and O, which constituted a selection of the explosives, the illicit drugs and miscellaneous everyday materials. Presently, the X-ray radiography was the technique used in the majority of the inspection systems. The conventional X-ray techniques generally measured the apparent density and shape of objects [3]. As a result, these X-ray

inspection systems were well suited for detecting the metallic objects with the readily identifiable shapes such as the firearms and other weapons. However, they were less well suited for detecting the illicit substances that had similar densities and shapes to many common substances [4-6]. On the other hand, since the neutrons can easily penetrate the high atomic number materials but react significantly with the low atomic number materials, the method used to detect these contrabands based on neutron radiography then was of interest. Figure 1.2 showed the mass attenuation coefficients for thermal neutron and gamma rays as a function of atomic mass of elements.

The neutrons were classified according to their energy. Generally, the neutrons can be roughly classified as the cold, the thermal, the epithermal and the fast neutrons. The thermal neutron radiography which utilized the thermal neutron had been thoroughly developed and was commercially available. This stemmed from the availability of the high-intensity thermal neutron beams generated from the nuclear research reactors and the radioisotopes neutron sources [8]. However, due to the high installation cost, the safety concern and the immobility of the research reactors, a portable neutron generator was chosen as the neutron source. In additional, the neutron generators had the essential advantages over the radioisotope neutron sources. For example it was possible to control of the neutron flux and its time parameters. The operation and transportation were relatively simple as there was no neutron emitted when they are switched off [9].

Since the neutrons generated from a portable neutron generator were mostly the fast neutrons, the system was emphasized on using the fast neutrons for the purpose of conducting the radiography. The fast neutron radiography had the advantages due to the less diffusive nature of the fast neutrons. Particularly, the fast neutrons were suitable for detecting for defects in low-Z materials shielded by thick, high-Z parts [10]. On the contrary, the thermal neutrons were less capable of penetrating thick objects due to the high probability of their interacting with the material's nuclei [11].
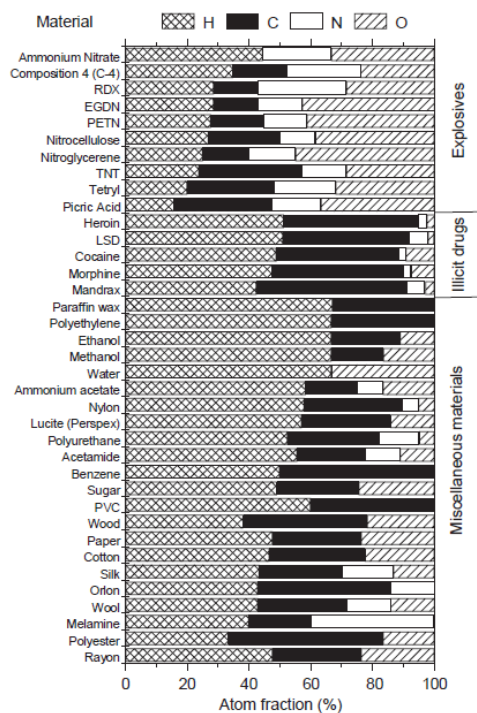
Figure 1.1 The atomic fractions (as a percentage) of the elements H, C, N and O, which constitute a selection of explosives, illicit drugs and miscellaneous everyday materials [2]
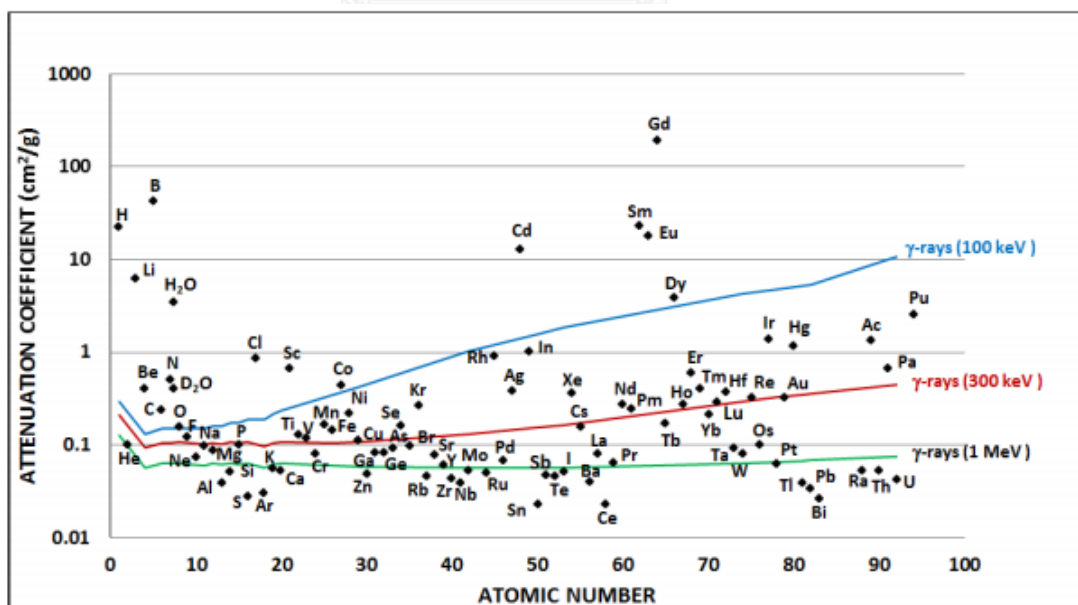
Figure 1.2 The mass attenuation coefficients for thermal neutron and gamma rays as the functions of the atomic mass of elements [7]

1.2 Neutron Radiography

The neutron radiography had been around since the first research reactors became available in 1950s and had grown in use and application throughout that time. Due to the increasing availability of high intensity thermal neutron beams from the nuclear research reactors and from the neutron sources in recent years, the thermal neutron radiography had become a well-accepted inspection technique [12].

Similar to the X-ray radiography, the neutron radiography utilized the transmission of the radiation to obtain the information on the structure and/or the inner processes of a given object. The object under examination was placed in the path of the incident radiation, and the transmitted radiation was detected by a two-dimensional imaging system [13].

The three main components for the neutron radiography were a neutron source, an object/sample and a detector. The important considerations involved the intensity of the neutron source, the spectrum of neutron energies, the collimation of the neutron beam and its time structure. Figure 1.3 illustrated the interaction of a neutron beam through the object and the detector [14].
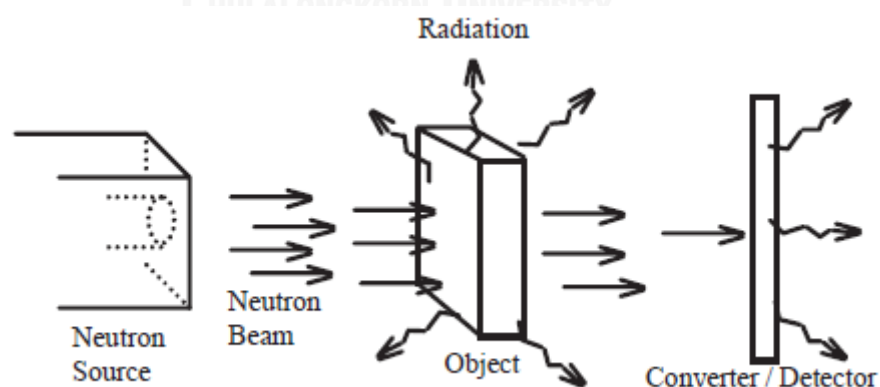
Figure 1.3 The schematic diagram for the neutron radiography [14]

There were three types of neutron sources, i.e., the research reactors, the radioisotopes neutron sources and the electrically induced fusion neutron sources.

Among all three, the research reactors were the most commonly used neutron sources. The fast neutrons emitted by the fission reaction of uranium-235 (^{235}U) were slowed down by the moderator to become thermal neutrons. By using the collimator, the high intensity, uni-directional thermal neutron beams, free from the interference by the gamma radiation could be produced. As a result, the excellent image quality could be obtained within short exposure time.

The isotopic neutron sources were the radioisotopes that underwent the spontaneous fission such as californium-252 (^{252}Cf) or the indirect reaction such as americium-241/beryllium (^{241}Am/Be), where the neutrons were emitted due to bombardment of Be by the alpha particles produced by ^{241}Am. The neutron flux for the radioisotopes neutron source was low and, therefore, a longer exposure time was required to obtain the good quality images.

The electrically induced fusion neutron sources were the particle accelerators or the neutron generators, which emitted neutrons produced by the nuclear reaction. The incoming particles such as ^{1}H and ^{2}D were accelerated and brought to hit the target nuclei to produce neutrons. The energy produced by these nuclear reactions was monoenergetic. Depending on the design of the neutron generators, the strength of the output could be up to 10^{12} neutrons per second.

The detector was a device to record the radiation intensity information associated with the neutron beam transmitted through the object. The commonly used detectors were the films, the imaging plates and the optical cameras. In case of the neutron radiography, a converter was necessary to produce the signal that could be recorded by the detector. The commonly used neutron converter screen/imaging recording devices were summarized by N. Chankow as below [7];

i.   Metallic foil screen/film: The metallic foil with the high neutron cross section was employed to convert the neutrons to the beta particles, the gamma rays and/or the conversion electron that could be detected by

the x-ray film. Gadolinium (Gd) foil was the best metallic screen for the neutron radiography due to its high absorption cross section. In this case, the imaging plates could also be used as the recording devices instead of film.

ii.   Light emitting screen/film: The light-emitting screen was a mixture of the scintillating materials or phosphor with lithium-6 (^{6}Li) and/or boron-10 (^{10}B). In this case, the neutrons interacted with ^{6}Li or ^{10}B produced alpha particles via (n,α) reaction. The light was then emitted from the energy loss by the alpha particles in the scintillating materials or phosphor. The light sensitive film, the digital camera or the video camera could be then used as the recording devices. By using this technique, the real time radiography can be performed.

iii. Alpha-emitting screen/track-etch film: The converter screen was made of lithium and/or boron compound. The alpha particles emitted from (n,α) reactions then interacted with the track-etch film to produce the damage tracks along their trajectories. The detector was later etched by the chemical solution to enlarge the damage tracks. After the etching process, the damage tracks could be visible under an optical microscope with the magnification of 100 times or higher.

As the neutrons passed through an object, they interacted with the nuclei by the scattering and absorption. The probability of such events was an exclusive property and accounted for the unique radiographic information available with the neutron beams. The energy of neutron beam was another key factor that influenced the cross section of such interaction event. As a result, the neutron radiography with the different energy neutrons had the different features.

Generally, the lower neutron energy gave better image contrast, due to the 1/v behavior of the neutron capture cross-section. The thermal or cold radiography was suitable for the small organic samples with the thickness of several mm to a few cm. However, when the samples were thick and capable of absorbing most incident neutrons, the contrast and resolution of low energy radiography can be poor. By benefitting from the small absorption cross section, the fast neutron radiography had been used to investigate the thicker samples. However, the several MeV fast neutrons could be hard to detect due to their high penetration [15].

1.3 Problem Statement

As mentioned in the earlier part, the using of a neutron generator had plenty of advantages over the other neutron sources. However, due to the relatively smaller size of the machine, the neutron flux produced by the neutron generator was relatively small compared with that of research reactor. The fast neutron radiography was seemed to be an attractive non-destruction technique due to its high penetrating power. In the fast neutron radiography, the neutron energy spectrum, the imaging geometry, the neutron scattering and the position-sensitive detector influenced the feature contrast, resolution and the signal-to-noise ratio in the image [16]. At the same time, there were some difficulties on detecting the fast neutrons due to their absorption cross sections, which were normally much smaller than that of the thermal neutrons. Furthermore, a significant amount of X-ray also was produced during the operating of the neutron generators. This was due to the interacting of the deuterons and the nuclei of the target material instead of the coated tritium atom.

1.4 Objective

The objective of this study was to develop the basic configuration for the fast neutron radiography by using the portable neutron generator in order to provide an image of sufficient information with the low X-ray effect.

1.5 Scopes of the study

The scopes of this study were limited to the following criteria;

1. The research was conducted with the neutrons from a portable neutron generator (model Thermo Scientific MP 320).

2. The image plate to be used was BAS-ND2040 (Fuji). Some other image plates were also used for the comparison purpose.

3. The materials tested with were the normal household materials, which are mostly composed of C, H, N and O. If possible, some special materials such as urea fertilizer or kerosene might also be tested.

4. The metal sheet such as lead, steel and aluminum were to be used as the shielding and packaging materials. The typical paper, plastic, cloth and leather might also be used to simulate the baggage containing the sample to be tested.

5. The range of beam current and the HV were limited according to the specification of the portable neutron generator.

1.6 Literature Review

In comparison with the thermal neutron, a high intensity fast neutron source was much easier to obtain since no moderator was required. Compared to the thermal neutrons, there was very little attenuation among elements for the fast neutrons. This allowed the fast neutrons to penetrate the very thick materials. The fast neutron penetration did depend upon the nuclei density and, thus, the regions with the significant density variation such as the cracks and the voids could be imaged. Indeed, by comparing the linear attenuation coefficients of various materials for x-rays and neutrons, it is evident that the fast neutrons could penetrate some materials far more readily than the 10 MeV photons. In addition, the fast neutrons

retained their high absorption in the hydrogen bearing materials. Consequently, there would be some inspections that are ideally suited for fast neutron imaging [17].

The fast neutron radiography had been studied at the fast neutron source reactor YAYOI of the University of Tokyo since 1986. In 1999, Shigenori Fujine et. al. reported the development of the imaging techniques for fast neutron radiography in Japan [18]. The reported imaging techniques included the CR-39 track-etch detector, the electronic imaging system (television method), the direct film method, the imaging plate and also the fast and thermal neutron concurrent imaging method. Their results found that the track-etch method with CR-39 was insensitive to the gamma rays. The fluorescent converters, the films and the imaging plates had the same degree of sensitivity to gamma rays. For the static images, the track-etch, the TV and the film methods had the acceptable quality for the image analysis. They also concluded that the imaging plate and the Indium transfer methods had the capability for the fast neutron radiography, but a new imaging plate should also be developed.

The fast neutron profile measurements were required for the characterization and the application. A method for taking the fast-neutron profile had been developed by Toshiya Sanami et. al. using an imaging plate combined with a polypropylene converter [19]. The H(n,p) reaction was the most useful reaction to convert fast neutrons into charged particles with a large cross section for fast neutrons between a few MeV and 15 MeV. The imaging plates could detect both the gamma ray and the charged particles. By this method, the spatial distribution of the fast neutrons was obtained without any gamma ray contamination by taking the difference between the data with and without the converter. Figure 1.4 showed the detection scheme developed and its photo-stimulated luminescence (PSL) read out.
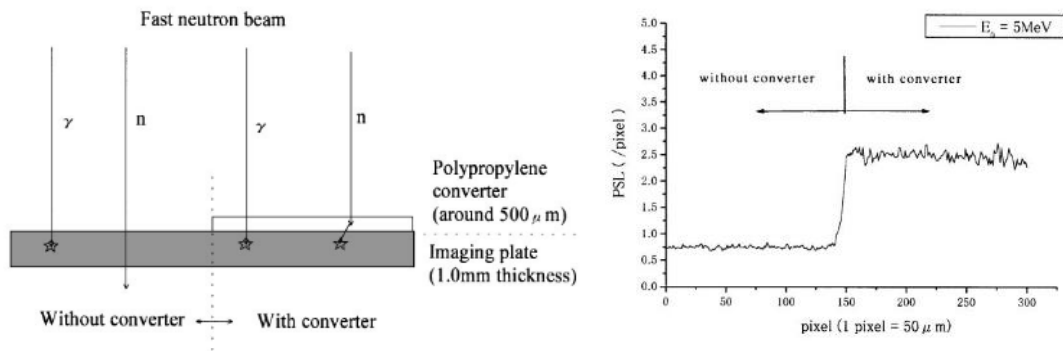
(a) Detection scheme by an imaging plate with a polypropylene converter

(b) The PSL profile of the imaging plate

Figure 1.4 The detection scheme developed by Toshiya Sanami et. al. and its PSL profile of the imaging plate

An experiment that studied the applicability of the image plate to the fast neutron radiography was performed by Masahito Matsubayashi et. al. [20]. They carried out the experiment at YAYOI reactor, University of Tokyo. The combination of the duplicate image plates and a piece of polyethelene sheet as a proton emitter was used to detect the fast neutrons and to discriminate the gamma rays associated with the neutron beams. The imaging plates used were the ^{3}H detection imaging plates produced by Fuji Photo Film Co. Ltd. The experimental results showed that the method could be applicable to fast neutron radiography with effective discrimination of gamma-rays. By subtracting the PSL values between the duplicate imaging plates with and without polyethylene sheet, fast neutron radiography images with effective gamma ray correction were obtained successfully. Figure 1.5 showed the arrangement of the detecting system by Masahito Matsubayashi et. al. and its PSL read out.
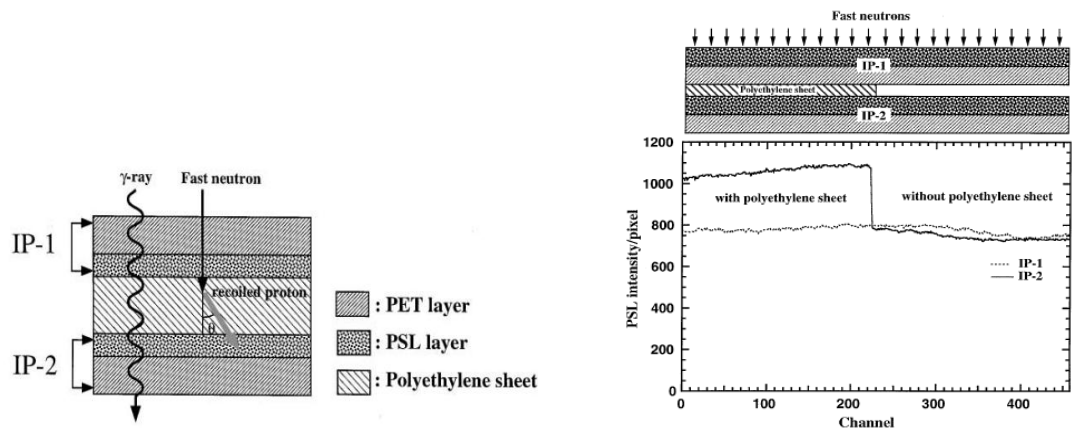
(a) The arrangement of the image plates and the polyethylene sheet for fast neutron radiography.

(b) Line profiles of IP-1 and IP-2 which were separated by a polyethylene sheet with half width of the IP.

Figure 1.5 The arrangement of the detecting system proposed by Masahito Matsubayashi et. al. and its results

Another research that investigating the use of the image plates as the detector in the fast neutron radiography was carried out by V. Mikerov et. al. [21]. The neutron source that they used was a portable 14 MeV neutron generator. They proposed two methods, i.e. "direct" and "transfer" method to enhance the neutron detection by the image plates (as shown in Figure 1.6). The result of the "transfer" method showed that this method was free form background noise but had a relatively low efficiency and thus required higher neutron flux. The "direct" method had higher efficiency but the image quality was affected by the background noise.
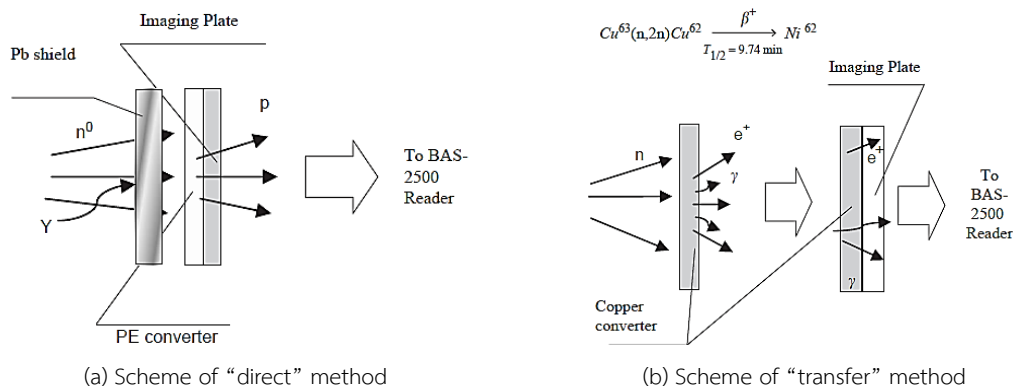
(a) Scheme of "direct" method

(b) Scheme of "transfer" method

Figure 1.6 The method of fast neutron radiography proposed by V. Mikerov et. al.

Nares Chankow et. al. studied the properties of a neutron imaging plate (NIP) and tested for its use in the non-destructive testing of materials [22]. The NIP that they used was BAS-ND2040 (Fuji). The study was carried out at Thai Research Reactor TRR-1/M-1. The results of the study showed that the PSL readout of the NIP is directly proportional to the exposure time and approximately 40 times faster than the conventional neutron radiography using Gd converter screen/X-ray film technique while the image quality of both technique are nearly the same.

จุฬาลงกรณ์มหาวิทยาลัย
CHULALONGKORN UNIVERSITY

CHAPTER 2

THEORY AND METHODOLOGY

As mentioned in previous chapter, in this study, the fast neutron radiography was carried by using the neutron generator while the imaging plate was used as the detector. In this chapter, more details on the theories, the configuration of the system and the procedure on how the research had been conducted were discussed.

2.1 Neutron generator

The neutron generators had been available for many years. The commercial deuterium-tritium (DT) generators could produce more than 10^9 n/s. The neutron generators could effectively be used for elemental analysis with neutron activation analysis (NAA) and prompt gamma neutron activation analysis (PGNAA). The conventional neutron generators had been shown to be effective for the applications including borehole logging, homeland security, nuclear medicine and the on-line analysis of aluminum, coal and cement. They were also effective for the analysis of the hidden materials by the neutron radiography.

Most of the neutron generators were designed to produce the neutrons by the deuterium–deuterium (DD) (at 2.5 MeV) or deuterium–tritium (DT) (at 14 MeV) reactions. The following equations show the DD and DT reactions.

$$^2\text{H} + {}^2\text{H} \longrightarrow {}^3\text{He} + {}^1\text{n} + 3.266\text{MeV}$$
$$^2\text{H} + {}^3\text{H} \longrightarrow {}^4\text{He} + {}^1\text{n} + 17.586\text{MeV}$$
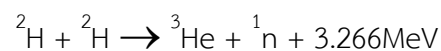
2.1.1 The operation of neutron generator
The most widely used and available generators were based on Penning Ion Source technology. This type of neutron generators was able to run in either continuous

mode or pulsed mode. The commercially available DT neutron generators range in yield from 10^7 to 10^{10} n/s, while those with DD range from 10^5 to 10^8 n/s [23].

The basic design of a modern compact Penning diode neutron generator consisted of a source to generate positively charged ions and a diode structure to accelerate the ions (usually up to ∼110 kV) to a metal hydride target loaded with deuterium, tritium, or a mixture of the two. Figure 2.1 illustrated the internal structure of the Penning diode neutron generator. A gas control reservoir, attached to the tube and made of a metal hydride material, was used to store the gas. The most common ion source used in neutron generators was a cold cathode, or Penning ion source, which was a derivative of the Penning trap, used in the Penning ion gauges. This simple ion source consisted of a hollow cylindrical anode (usually biased with 1–2 kV) with cathode plates at each end of the anode, usually at ground potential. An external magnet was arranged to generate a coaxial field of several hundred gauss within the ion source.
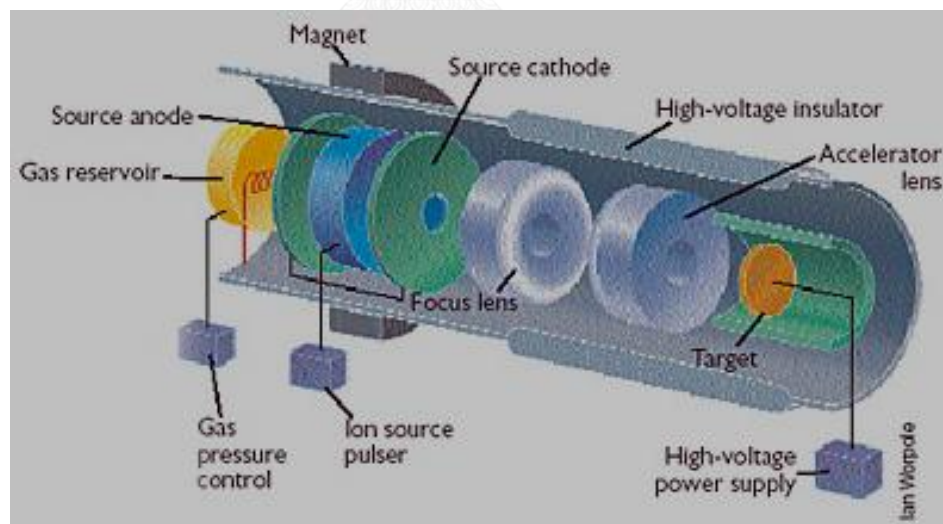
Figure 2.1 A schematic illustration of the internal structure of a compact neutron generator [23]

When the deuterium and/or the tritium gas was introduced into the anode at a pressure of about 0.1 Pa (10^{-3} Torr), the electric field between the anode and

cathodes ionizes the gas. An electron confinement was established in this plasma because of the orientation of the electric and magnetic fields, which forced the electrons to oscillate back and forth between the cathode plates in the helical trajectories. Although some low energy electrons might have lost their tracks and struck the anode, which created more secondary electrons, most would have remained trapped and ionized more gas molecules to sustain the plasma. The ions were not similarly trapped and could escape the chamber into the accelerating section of the tube through a hole at the center of one of the cathodes, the exit cathode.

2.1.2 The factor affecting neutron yield

The yield of the neutron reactions was mainly affected by two parameters, i.e., the high voltage and the beam current. The neutron yield for the DD and DT reactions was given in Figure 2.2. The total yield, F of neutrons produced in a nuclear reaction was given by

$$F = N\sigma\Phi$$

where F was the neutron yield per second, N was the number of target nuclei per square centimeter of target, σ was the reaction cross-section in cm^2 and Φ was the incident particle rate per second. The incident particle rate, Φ could be expressed in terms of beam current by

$$\Phi = I/C$$

where I was the beam current and C was the charge of the particle.
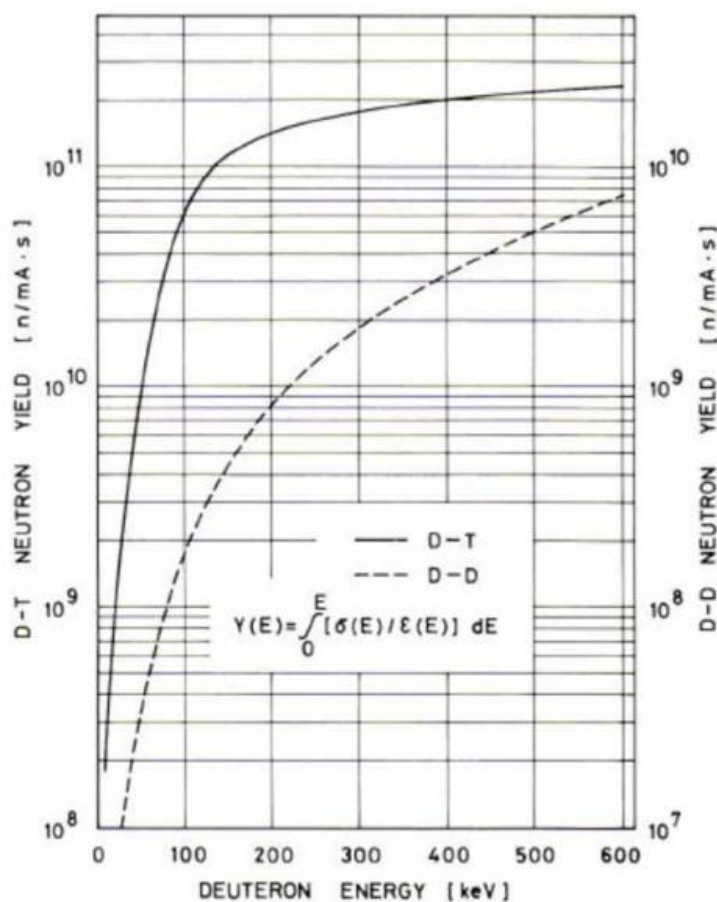
Figure 2.2 Neutron yields for DD and DT reactions as the functions of deuteron energy [23]

2.1.3 Neutron generator used in this study

In this research, the neutron generator used was the portable-typed DT neutron generator (model MP320) manufactured by Thermo Fisher Scientific. The neutron and the X-ray yield of this neutron generator were studied by varying the high voltage and the beam current. The results of the study were reported and discussed in the following chapters. Table 2.1 showed the technical specifications of this neutron generator [24].

Table 2.1 Technical Specification of Thermo Scientific MP320 Neutron Generator

Neutron Yield	1.0E+08 n/s
Neutron Energy	14 MeV
Pulse Rate	250 Hz to 20 k Hz, continuous
Duty Factors	5% to 100%
Minimum Pulse Width	5 μsec
Pulse Rise Time	Less than 1.5 μsec
Pulse Fall Time	Less than 1.5 μsec
Maximum Accelerator Voltage	95 kV
Beam Current	60 μamps
Power Supply	Integral
Neutron Module	12.07 cm X 57.15 cm
Control Module	Integral, Digital
Remote Control	RS-232/RS-485
Total Weight	12 kg
Safety features	√ Keylock: on/off √ Emergency: on/off √ Normal-open and normal-closed interlocks √ Pressure switch

2.2 Imaging plates

The imaging plate was a film-like radiation image sensor based on the photo-stimulated luminescence (PSL) phenomenon. This phenomenon involved a substance that re-emitted the light upon the second stimulation by the light with the wavelength longer than the luminescence wavelength of the first stimulation, the initial exposure. The imaging plate consisted of a specifically designed composite structure that traps and stores the radiation energy. A polyester support film was

uniformly coated with a photo-stimulatable luminescent material, and was then re-coated with a thin protective layer (as shown in Figure 2.3). The photo-stimulatable luminescent materials were the very small crystals (grain size: about 5 μm) of the photo-stimulable phosphor made of barium fluorobromide with the trace amount of bivalent europium as a luminescence center, formulated as BaFBr: Eu2+. The stored energy was stable until scanned with a laser beam whereupon the energy was released as luminescence [13].
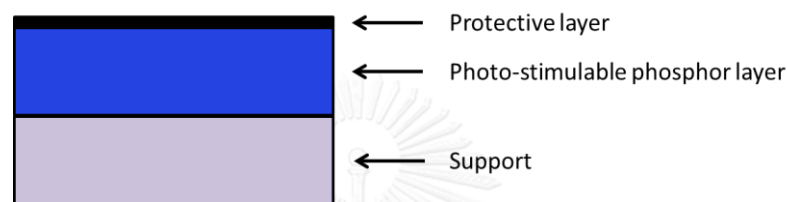
Figure 2.3 The composite structure of the imaging plates

The imaging plates were not only applicable in the medical and the industrial radiography, but also in many fields such as autoradiography, X-ray diffraction experiments, and transmission electron microscopy. In each case, the inherent imaging principle was the same. After the radiographic image had been transferred to an imaging plate, it was scanned point-by-point by a laser beam in an image reader. A series of the PSL emissions corresponding to the scanned pixels was then detected by a photomultiplier tube through a high-efficiency light guide. Figure 2.4 showed the radiation image reading process of the imaging plates. These analog signals were logarithmically amplified and converted into the digital signals. By processing these signals through a computer, the computed radiograph could be reconstructed [25]. The digital image allowed it to be possible for the post process analysis, such as filtering (for noise reduction), rendering (for the reconstructions), windowing (for the change of intensity scales), zooming and edge sharpness.
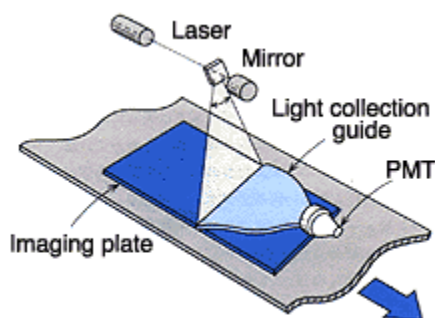
Figure 2.4 The principle of reading the radiation image from an imaging plate

The process of obtaining an image from the imaging plates was simple and chemical free. The imaging plate was the reusable image recording device. The imaging plate could be cleared by erasing the residual latent image with the uniformly irradiated visible light. Due to these advantages, the photographic films have been widely replaced by the imaging plates. Besides this, the imaging plate had the detection efficiency similar to that of the film but the response to the exposure was linear, and the dynamic range was almost four orders of magnitude broader (see Figure 2.5). In Figure 2.5, the "IP" was imaging plate while the "au" stated for arbitrary unit. Despite the spatial resolution (5–15 lines/mm) being lower than that with the film, the linearity and the larger dynamic range increased significantly the contrast [26]. The required exposure time of the imaging plates was also lower than that of the film. Guohai Wei et. al. reported that, under the same experiment condition, the neutron radiography based on the imaging plates required two-fifth of the time needed for the film method [27].
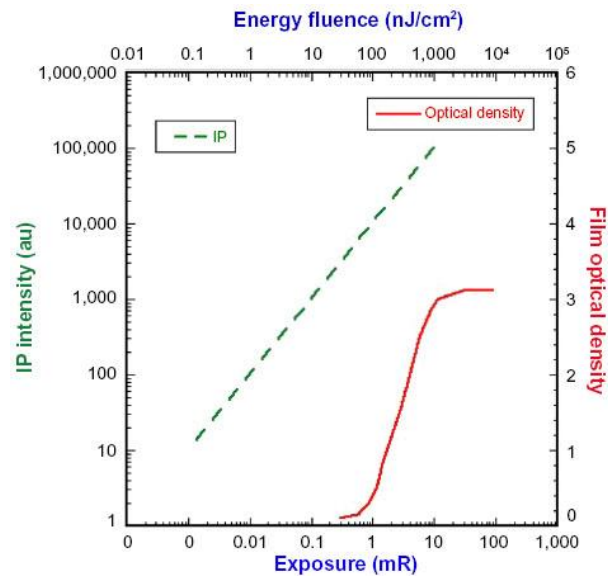
Figure 2.5 Response of film (red curve) and image plate (green curve) versus exposure (or energy fluence) [26]

2.2.1 Neutron imaging plate

The neutron imaging plate is the imaging plate that could be used for detecting the neutron without using the metal foil as the converter. The neutron imaging plates were made up by the thin layers consisting of a mixture of the storage phosphor, the neutron converter and the organic binder coated on a polymer film. Table 2.2 listed the cross sections of several isotopes which could be used for the converting the thermal neutrons into the different types of the secondary radiation. They could be applied in the form of the different compounds, which should be transparent. They were also available in the form of the fine powdered material, with a grain size in the order of a few micrometers [28].

Table 2.2 Conversion reactions of various isotopes for thermal neutrons (λ=1.8 Å) which have the potential to be used for the generation of the secondary radiation in the neutron sensitive imaging plates [28]

Reaction	Cross section (barn)	Emitted secondary radiation and freed energy (MeV)	Natural abundance
^{6}Li$(n,α)^3$H	940	α (2.05), ^{3}H (2.74)	7.5%
^{10}B$(n,α)^7$Li	3837	α (1.47), ^{7}Li (0.83) (93% of all reactions)	18.8%
^{155}Gd$(n,γ)$	60 900	Conversion electrons (0.04→0.200), γ-rays (up to 7.5 MeV)	14.8%
^{157}Gd$(n,γ)$	25 4000	Conversion electrons (0.03→0.182), γ-rays (up to 7.5 MeV)	15.7%
$_{64}$Gd$(n,γ)$	48 890	Conversion electrons (0.03→0.200), γ-rays (up to 7.5 MeV)	100%
^{235}U fission	583	Fission products (≅80)	0.72%

In 1994, Nobuo Niimura et. al. had developed two kinds of imaging plate neutron detectors, where the neutron converters, ^{6}Li and Gd were mixed with PSL materials on a flexible plastic support. The dynamic range and the spatial resolution of the developed neutron imaging plates were successfully obtained as 1:105 and less than 0.2 mm, respectively, which are comparable to the ones of the X-ray [29].

2.2.2 Neutron imaging plate used in this study

The neutron imaging plate used in this study was BAS-ND 2040 produced by Fuji Photo Film Co., Ltd.. This neutron imaging plate adopted Gd_2O_3 as the neutron converter and the ratio of the neutron converter and the photo stimulable phosphor was 1:1 [30]. The dimension of the imaging plates was 20 cm X 40 cm. The imaging plates were analyzed by the Fluorescent Image Analyzer FLA-5100 produced by Fuji Photo Film Co., Ltd.. The image plates were read by 635nm laser at 8-bit depth (0-255) and with the resolution of 100 μm/pixel.

2.3 Detecting system of the fast neutron radiography

As previously mentioned, the neutron generator emitted X-ray when the deuteron interacts with the nuclei of the target plates. Since the neutron imaging plates were not only sensitive with the neutrons but also the X-ray, the effect of X-ray must be reduced. For this purpose, the idea of combining two identical imaging plates, proposed by Masahito Matsubayashi et. al. [20], was adopted and modified for this work.

In this work, a combination of a shielding material sandwiched by two identical neutron imaging plates was employed as the detecting system for the fast neutron radiography. The shielding material chosen was expected to either shield yjr neutrons or the X-ray. As a result, the image obtained by the upper and the lower image plates were then differentiable.

Two shielding materials were suggested. The first one was lead which effectively attenuated X-ray. The other one was a piece of the acrylic sheet. The experiment was carried out to study the lead sheet as the shielding materials and it turned out that the lead sheet was not suitable. More details on this were discussed in chapter 3 of this thesis.

The acrylic referred to a family of the synthetic, man-made, plastic materials containing one or more derivatives of acrylic acid. The most common acrylic plastic was the polymethyl methacrylate (PMMA). The methyl methacrylate was the basic molecule, the monomer, from which polymethyl methacrylate and many other acrylic plastic polymers were formed. The chemical notation for this material is $CH_2=C(CH_3)COOCH_3$ or $C_5H_8O_2$. With the assumption that the X-ray could easily penetrate the light elements, by adding a thin acrylic plate as the shielding material between two imaging plates, the X-ray intensity remains the same for both imaging plates while the fast neutron intensity was reduced before reaching the second imaging plate (refer to Figure 2.6). The different results provided by the first imaging

plate (IP1) and second imaging plate (IP2) could provide the information regarding the effect from the fast neutrons.

X-ray   Fast neutron

IP 1

Acrylic

IP 2
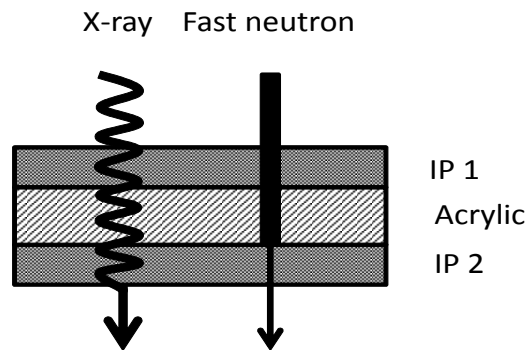
Figure 2.6 The schematic diagram for the detecting system used in the fast neutron radiography system and the induced effect

2.4 Binary operation for extracting the fast neutron information

Since the images were stored in digital form, a binary operation could be performed to extract the information. The Exclusive OR (XOR) operation was then proposed to extract the information from two imaging plates. With the XOR operation on the 1-bit (true/false) information, the result was true (binary = 1) only when the two inputs were different from each other, otherwise false (binary = 0) would be resulted. In other word, the combination of two images by the XOR operation should show up the pixels where the imaging plates contained the different information. Figure 2.7 illustrated the XOR operation between two black and white (1-bit) images. With the white color being represented as 1 and the black color as 0, the result of XOR operation showed the white circle which appeared only in Image 1 while the rest of the image was changed to black.

Image 1   Image 2   The result of XOR operation
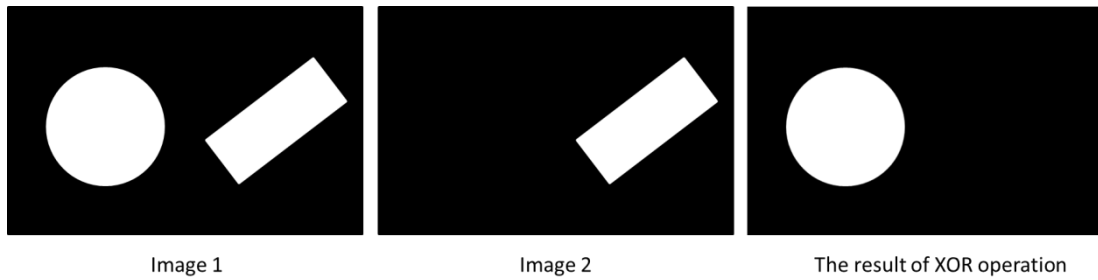
Figure 2.7 The XOR operation between two black and white (1-bit) images

Based on Figure 2.6, the imaging plates, IP1 and IP2, were expected to have the same information for X-ray but the different information for fast neutron since the acrylic would have attenuated and diffused the fast neutrons. Compare with Figure 2.7, if the rectangular shape was the result from the exposure to the X-ray where as the circle was the result from the neutron exposure, by using XOR operation, the final result would show only the effect of the neutron exposure. As a result, the neutron information could be obtained where as the effect of the X-ray produced by the neutron generator could be eliminated.

As the image obtained from the image plate reader was of 8 bit depth, the image was actually gray in color. In this case, the absolute black was represented by 0 and the absolute white was represented by 255. There was the different degree of grayness lay in the range between 1 and 254. The XOR operation would be calculated according to bit per bit in parallel. The XOR operation on 8-bit depth image was illustrated as in Figure 2.8.

Image 1   Image 2   The result of XOR operation
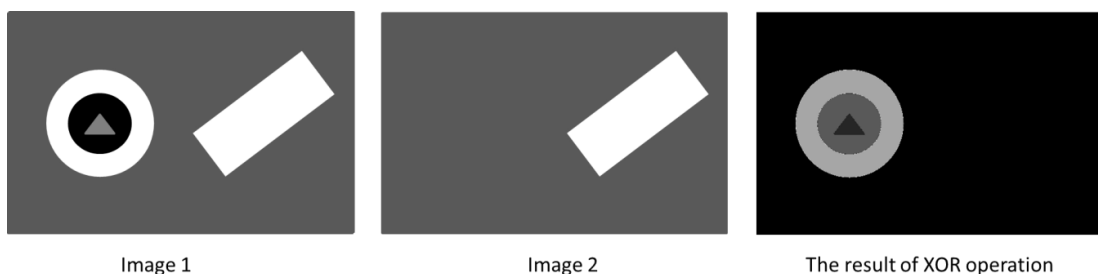
Figure 2.8 The XOR operation between two 8-bit depth images

In 8-bit depth images, the XOR operation turned the result to black (0) if two input values were the same. The larger difference would induce a whiter result whereas the smaller difference resulted in the darker pixel. Generally, the difference in the higher bit resulted a whiter pixel while the difference in the lower bits gave a blacker pixel.

2.5 System configuration and procedure for the fast neutron radiography

Figure 2.9 showed the schematic configuration of the fast neutron radiography system. In order to obtain a radiograph with the good sharpness, the distance between the source and the detecting system was kept long where as the distance between the sample and detector was kept as close as possible. The sample was placed normal to the window of the neutron generator, which indicated the direction of the neutron beam.

No collimator was used in the fast neutron radiography system. The use of a collimator could enhance the image quality. However, due to the low neutron intensity produced by the neutron generator, it was necessary to prevent the loss of the neutrons due to the use of the collimator.
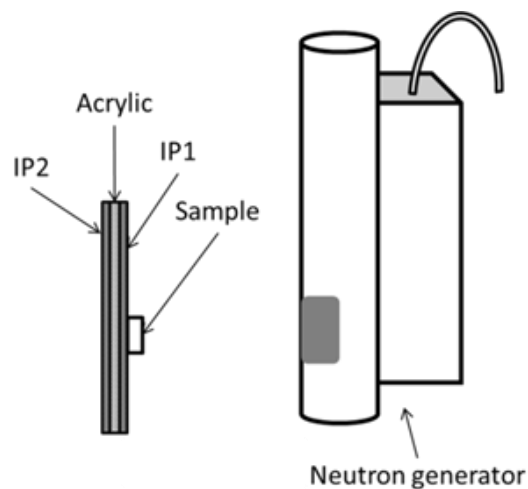
Figure 2.9 The schematic diagram for the fast neutron radiography system

After exposing the sample and image plates for a preset time, the imaging plates were immediately read by the imaging plate reader. As the imaging plate reader could not scan both imaging plate at the same time, one imaging plate was kept in a dark area to avoid exposing to light while another imaging plate was scanned. After the reading, the imaging plates were cleared for the next measurement. All of the measurements should be repeated at least twice to confirm the reproducibility of the measurements.

2.6 Image processing

The data of imaging plates were stored in the special file format after the scanning of imaging plates by the Fluorescent Image Analyzer FLA-5100. This file format could only be opened, edited and analyzed by the software called "Multi Gauge". In order to do the XOR operation, the images were exported to the BITMAP files, which could be read by other software. The exported images were saved as the color BITMAP files [31].

BITMAP was the native graphic format for Windows. BITMAP encoded the color information by using 1, 4, 8, 16, or 24 bits for a pixel. The bits-per-pixel count, also known as the image's color depth, determined the maximum number of color levels an image might have. An 8-bits per pixel could have 256 colors, for example. BITMAP contained four main sections; a bitmap file header, a bitmap info header, a table of color values, and the bitmap data itself. The bitmap data with the extension "RLE" was the BITMAP information compressed by the RLE method. However, the compression of the BITMAP data was rare [32]. The BITMAP file format was chosen because it was simple and could be read by most softwares.

The combination of two images by the XOR operation was done by using a software called "ImageJ", a public domain Java image processing and analysis program inspired by NIH Image for the Macintosh [33]. Both images from the first and second imaging plates were the raw images which were exported by the "Multi

Gauge" without any adjustment of contrast or brightness. However, the alignment of the images must be conducted so that the XOR operation could be performed by "ImageJ" correctly.

Some attempts also were carried out to improve the resulted images by adjusting the brightness and the contrast prior to the XOR operation. The brightness controlled the level of light intensity in the image where as the contrast represented the range between the darkest pixel and the lightest pixel. Figure 2.10 illustrated how the adjustment of the brightness and the contrast affected the distribution curve of an image. As shown in Figure 2.10, by increasing the brightness, the whole distribution curve would shift to the lighter side and as a result, the overall image could become whiter. On the other hand, the adjustment of contrast could increase the range between the minimum and maximum gray value among the pixels. The pixels which were relatively darker would become even darker while the relatively lighter pixels would become brighter. In this study, the brightness and contrast adjustment were done by using the software "Microsoft Office 2010".
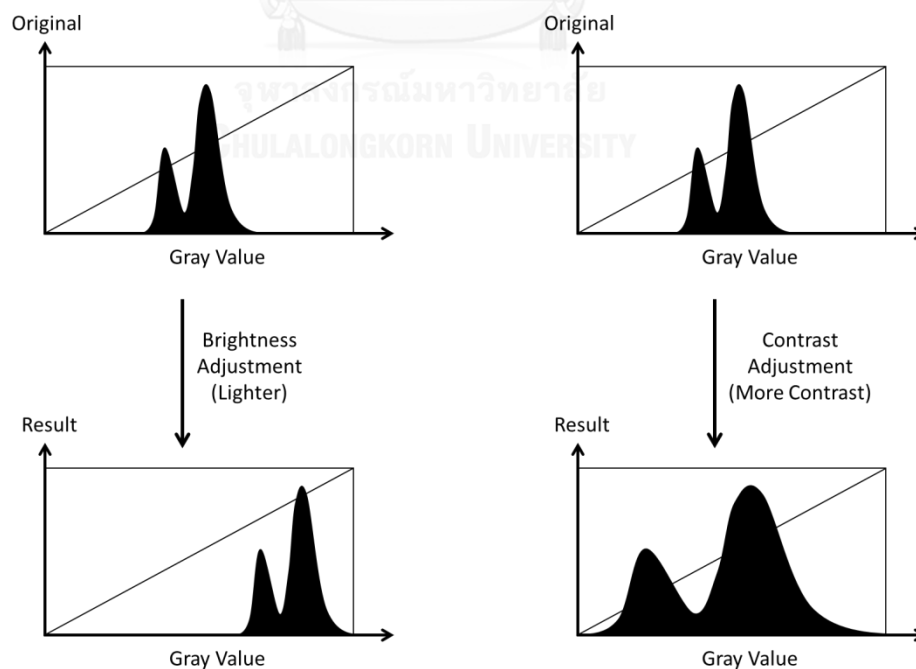
Figure 2.10 The change of distribution curve of an image by adjusting the brightness and the contrast

CHAPTER 3

EXPERIMENTS AND RESULTS

Two preliminary studies were done to figure out the basic configuration to be implemented for the fast neutron radiography. The first of them was to study the profile of the neutron generator regarding the production of the neutron and the X-ray yield at various beam currents and high voltage settings. The second one was to consider the shielding material to be inserted between the first and second imaging plates.

The basic fast neutron system configuration that was employed used the acrylic plate as the shielding materials and the fast neutron information were extracted by conducting XOR operation. Three basic samples (water, paraffin and plasticine) with the different combinations of packaging materials were used to test the system. The fast neutron radiography system was then used to test the "unknown" samples which simulate the illicit substance like the explosives and the flammable liquid. The results from the measurement were shown in this chapter. Meanwhile, the detail on the configuration of the system was discussed.

After all the experiments, a post experiment study which studied the improvement of the image quality was carried out by adjusting the contrast and the brightness.

3.1 Preliminary Study 1: Study on the profile from the neutron generator

The profile of neutron generators was obtained by plotting the neutron yield and the X-ray yield produced according to the different setting of the neutron generator parameters. A boron-lined proportional counter was used to determine the neutron counts while a Geiger-Muller gas-filled (GM) counter was used to determine X-ray counts. Figure 3.1 illustrated the setup of the experiments. The experiments were

carried out twice for the same settings; the counting time was set at 2 minutes and 6 minutes respectively. Due to the length of time needed to transit for the different locations of the detecting systems from the control panel of the neutron generator, the counting time was set one minute longer than the actual operating time for the neutron generator.
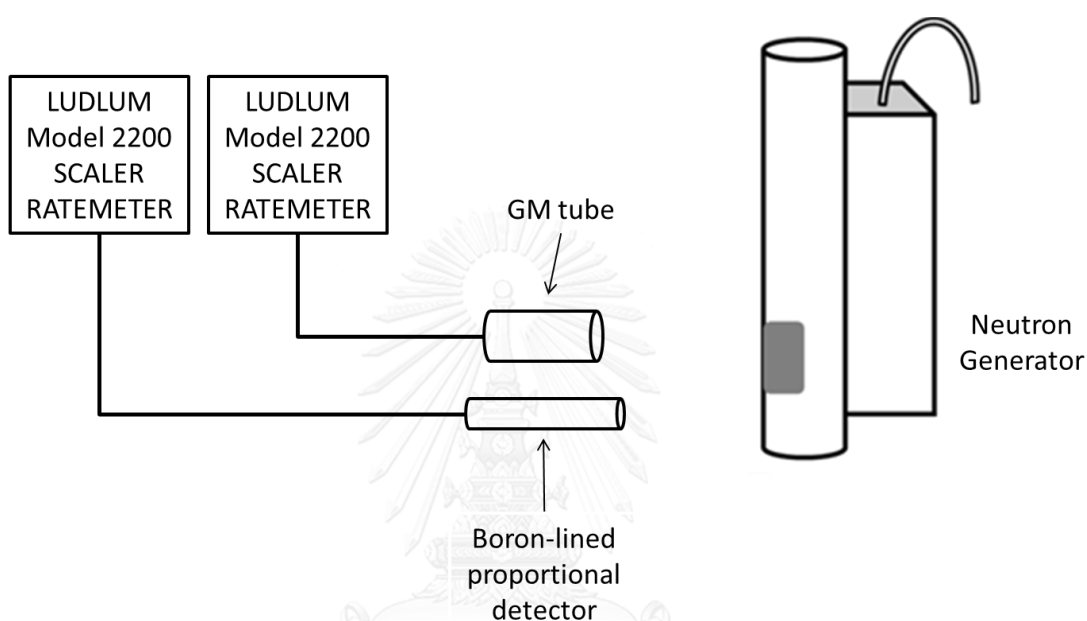
Figure 3.1 The schematic diagram of the experiment set up for the preliminary experiment 1

Table 3.1 and Table 3.2 showed the neutron count rate and the X-ray count rate respectively. The largest uncertainty for the data obtained was 20.16%. This was due to the low count rate for X-ray at the lowest beam current (20 µA) and at the high voltage of 40 kV. On the other hand, the lowest uncertainty obtained for the data was 0.54%. This value was obtained for the neutron count at the high voltage of 75 kV and the beam current 70 µA. The net count rate was 7210.4 ± 38.83 cpm.

Table 3.1 The net neutron count rate (cpm) detected by the boron-lined
proportional counter

HV (kV)	Current (µA)					
	20	30	40	50	60	70
40	176.2 ± 10.64	245.7 ± 11.46	328.7 ± 12.33	398.7 ± 13.00	494.9 ± 13.84	508.0 ± 13.95
45	308.0 ± 12.12	446.2 ± 13.42	557.2 ± 14.35	655.0 ± 15.11	815.7 ± 16.25	906.7 ± 16.85
50	460.2 ± 13.55	664.9 ± 15.18	875.4 ± 16.65	1041.0 ± 17.69	1243.5 ± 18.87	1437.9 ± 19.92
55	687.4 ± 15.35	1010.0 ± 17.50	1301.9 ± 19.19	1608.4 ± 20.78	1939.7 ± 22.35	2137.7 ± 23.23
60	938.7 ± 17.06	1408.0 ± 19.76	1889.7 ± 22.12	2269.0 ± 23.78	2720.2 ± 25.60	3079.7 ± 26.94
65	1252.0 ± 18.92	1954.9 ± 22.42	2546.4 ± 24.92	3103.5 ± 27.02	3769.0 ± 29.31	4254.9 ± 30.86
70	1639.9 ± 20.94	2511.5 ± 24.78	3341.7 ± 27.87	4086.5 ± 30.34	4894.9 ± 32.78	5661.9 ± 34.91
75	2078.5 ± 22.97	3157.0 ± 27.22	4188.9 ± 30.66	5289.2 ± 33.89	6274.0 ± 36.52	7210.4 ± 38.83

Table 3.2 The net X-ray count rate (cpm) detected by the GM counter

HV (kV)	Current (µA)					
	20	30	40	50	60	70
40	55.5 ± 11.19	84.3 ± 11.58	105.7 ± 11.85	130.0 ± 12.15	157.5 ± 12.47	156.2 ± 12.45
45	103.2 ± 11.82	162.7 ± 12.53	180.0 ± 12.72	219.2 ± 13.14	252.3 ± 13.48	288.5 ± 13.84
50	164.3 ± 12.55	213.5 ± 13.08	298.0 ± 13.93	348.5 ± 14.40	402.7 ± 14.87	463.8 ± 15.29
55	242.7 ± 13.38	343.5 ± 14.35	452.2 ± 15.29	526.0 ± 15.88	637.0 ± 16.71	727.2 ± 17.35
60	329.3 ± 14.22	443.0 ± 15.22	638.3 ± 16.72	751.5 ± 17.51	885.7 ± 18.39	1001.0 ± 19.10
65	453.0 ± 15.30	644.3 ± 16.77	863.2 ± 18.25	1009.8 ± 19.65	1228.8 ± 20.40	1389.7 ± 21.26
70	538.8 ± 15.98	864.5 ± 18.26	1087.8 ± 19.61	1340.0 ± 21.00	1610.8 ± 22.17	1888.7 ± 23.66
75	731.5 ± 17.38	1153.8 ± 19.98	1391.5 ± 21.27	1793.5 ± 23.23	2117.2 ± 24.67	2431.5 ± 25.97

The results obtained were plotted as shown in Figure 3.2 and Figure 3.3. Figure 3.2 showed the neutron yield while Figure 3.2 showed the X-ray yield from the neutron generator. There was no significant difference between the curves of the neutron count rate and the X-ray count rate. At the low HV region (40-45 kV), the yields produced by all range of beam current were very close. The yields became significantly different at the higher HV region (started from 55kV). The curve of the higher HV tended to increase more exponentially compared with the lower HV.

The beam current represented the deuterons flow rate to the target. A higher beam current could produce more available deuterons. On the other hand, the high

voltage could affect the kinetic energy of the deuterons. As a higher voltage applied could accelerate the deuterons to a higher speed and thus more deuterons could initiate the fusion. Therefore, more neutrons were produced.
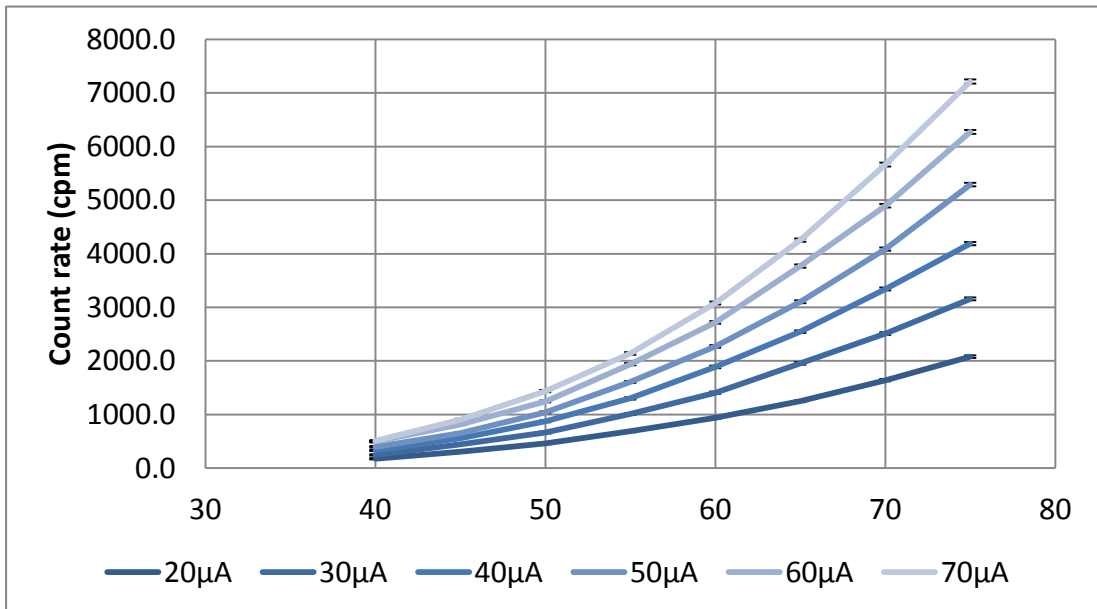
Figure 3.2 The graph of the neutron count rate against the high voltage applied on the neutron generator
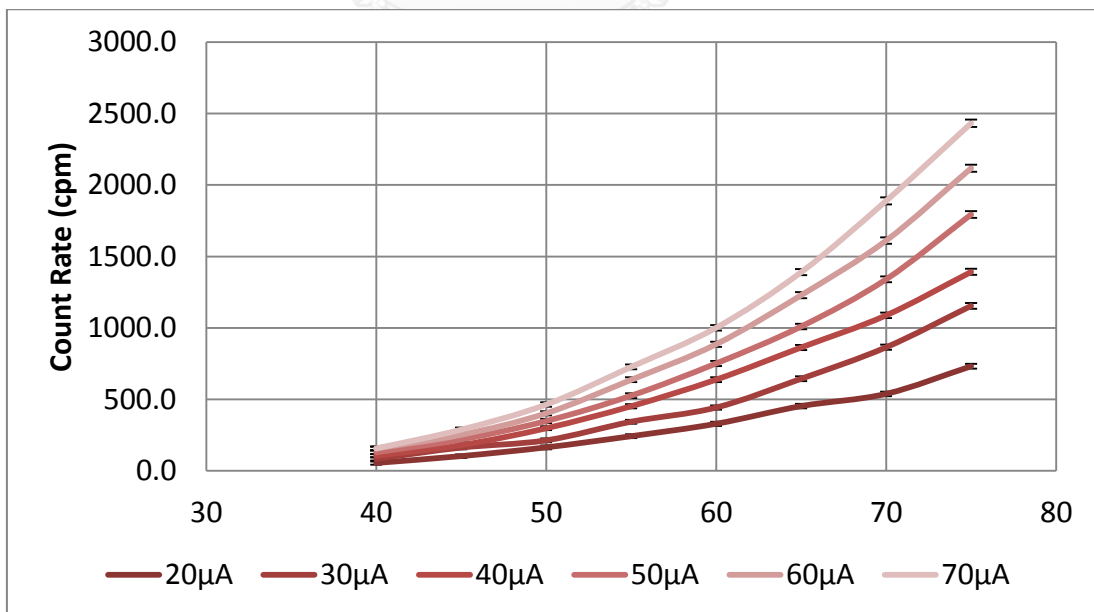
Figure 3.3 The graph of the X-ray count rate against the high voltage applied on the neutron generator

3.2 Preliminary Study 2: Study on the shielding effect of the lead sheet as the shielding material in the detecting system.

There were two experiments carried out during this preliminary study. One of them was to study the attenuation factor of the X-ray by the lead shield. The next one was to test if the lead sheet would be suitably used as the shielding material inserted between two imaging plates.

3.2.1 Experiment on the attenuation factors of lead sheet

The previous experiment showed that a significant amount of X-ray was produced during the operation of the neutron generator. An experiment was carried out to estimate the shielding effect of the lead sheets with the thicknesses of 1 mm, 1.5 mm, 2 mm and 3 mm. The shielding effect of the lead sheets with the thickness of 2 mm and 3 mm stacked up by the 1 mm lead sheets were also studied. A GM detector was used to detect the X-ray and it was put inside a thick lead column to shield off the x-ray that came from the other directions. The counting time of each measurement was set at 2 minutes. For this experiment, the neutron generator operated at the beam current of 60 µAmps and the high voltage of 75 kV. Figure 3.4 and Figure 3.5 showed the block diagram and the setup of the experiment.
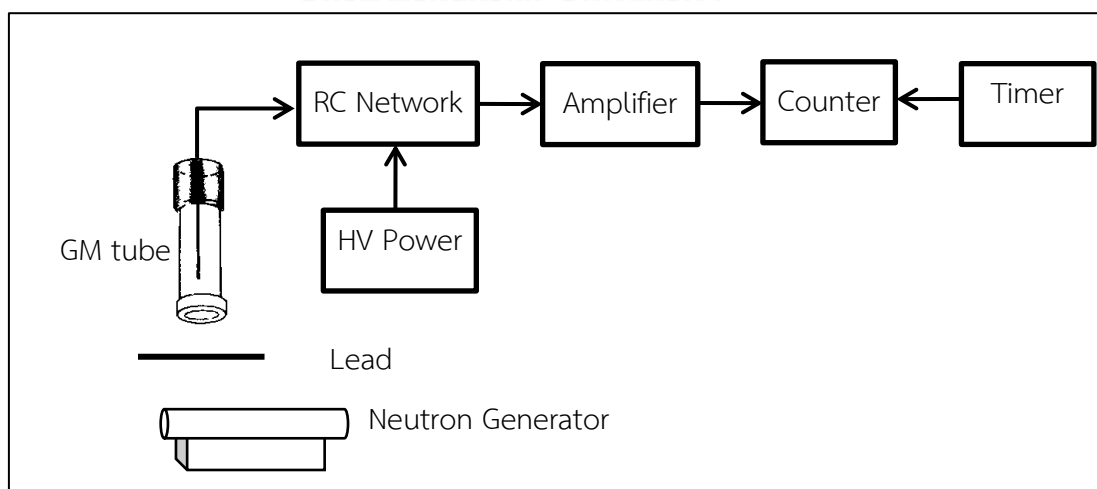
Figure 3.4 The block diagram of the experiment set-up for the preliminary experiment 2 part 1

(a) Experiment set-up · (b) Front view of detector · (c) Lead covered in front of detector
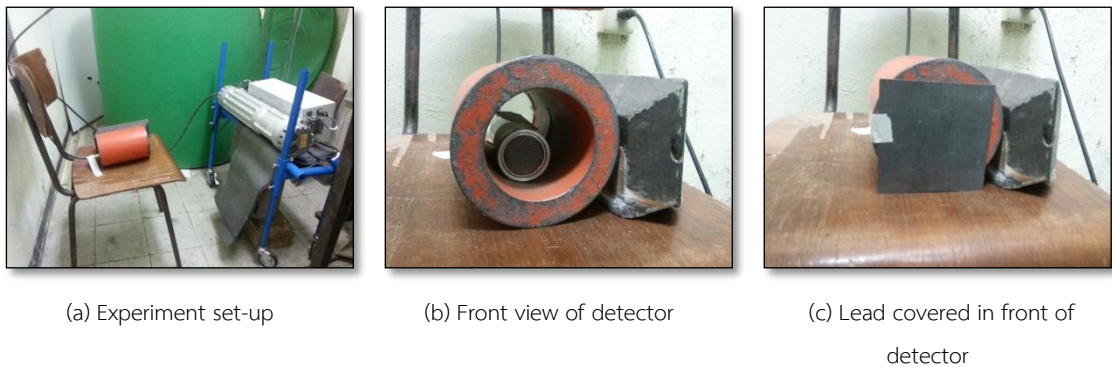
Figure 3.5 The set-up of the experiment for the preliminary experiment 2 part 1

The experiment was repeated twice and the results were shown in Figure 3.6. The results of both tests showed that the attenuation factor (Ix/Io) was decreased as the thickness was increased. Figure 3.7 showed the average value of both tests. The standard deviations of the readings were varied from 0.001% to 0.91%. The results of n plates thickness was slightly varied from the single plate with the same overall thicknesses. Based on the standard deviation obtained, the use of the single plate was better than the stack up of numbers of plates. From the results obtained, the x-ray intensity could be reduced by around 2.5% for every 1 mm increment on the thickness of the lead shield.
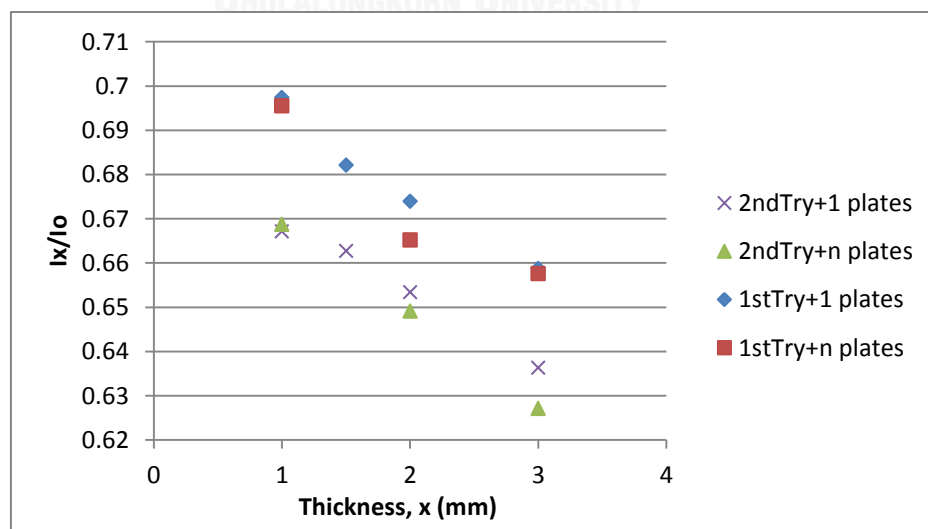
Figure 3.6 The attenuation factor (Ix/Io) against the thickness of lead sheet
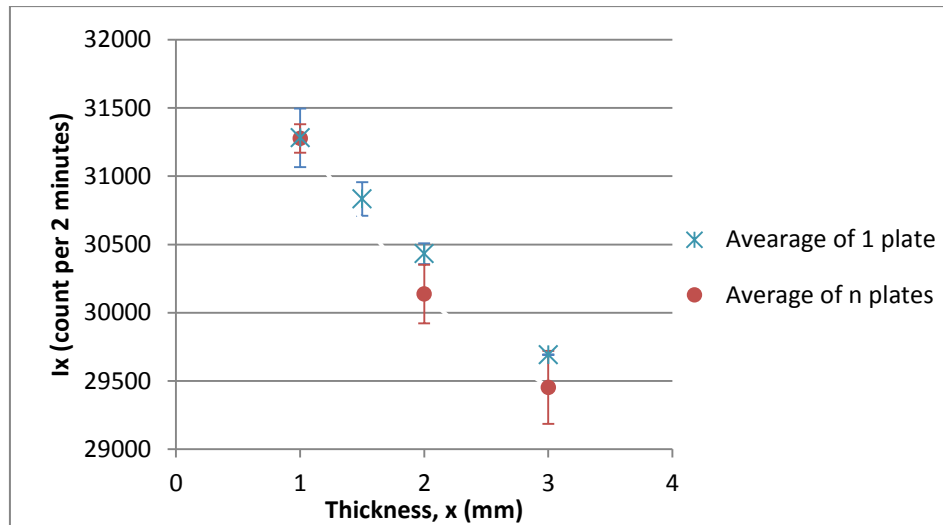
Figure 3.7 The average values of transmitted counts (Ix) from two sets of measurements

3.2.2 Experiment on using 1 mm lead sheet as the shielding material

The results in the previous experiment showed that, with the use of a lead sheet of 1 mm thickness, the intensity of X-ray detected by a GM counter could be reduced by 2.5% of its original intensity. In order to generate the difference in X-ray images, a 1 mm lead sheet was placed between the first imaging plate, IP1 and second imaging plate, IP2. Figure 3.8 showed the experimental setup of the system.

Figure 3.8 The experiment set up for the preliminary fast neutron radiography system with the use of lead sheet as the shielding material

In this experiment, the parameters of neutron generator were set as 60 µA and 75 kV. The exposure time for each measurement was 15 minutes. In this experiment, three samples were used, i.e., a lead collimator, a packet of water and a water packet placed in a metal box (see Figure 3.9).
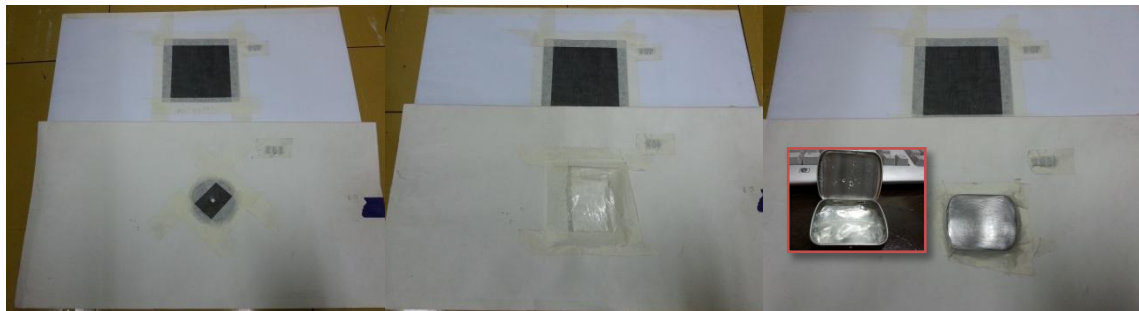
| (a) A pieces of lead collimator | (b) A packet of water | (c) A metal box with water packet |

Figure 3.9 The samples used to test the preliminary fast neutron radiography system

Figure 3.10 and Figure 3.11 showed the images resulted from the first imaging plate, IP1 and the second imaging plates, IP2 respectively. Apparently, the result from IP1 and IP2 had no similarities. As shown in Figure 3.10, with the use of lead sheet, all the radiation was prevented from reaching IP2. The radiation detection by the GM counter was incomparable to that of the imaging plates as the imaging plates were much more sensitive than the GM counter. From the results obtained, it was considered that the use of lead sheet as the shielding material was not suitable for this work.

| (a) A pieces of lead collimator | (b) A packet of water | (c) A metal box with water packet |

Figure 3.10 The result for the first imaging plates, IP1 from the preliminary fast neutron radiography system

| (a) A pieces of lead collimator | (b) A packet of water | (c) A metal box with water packet |
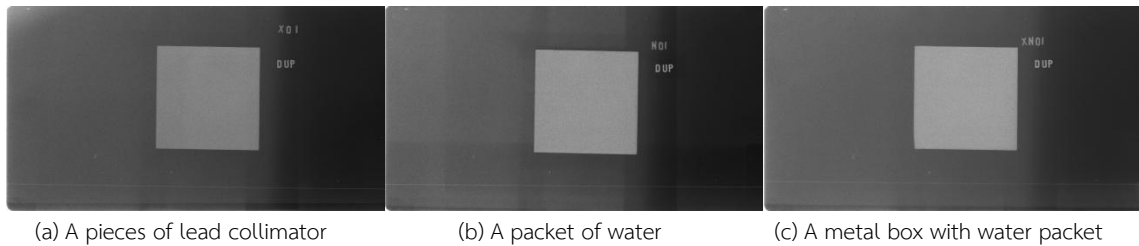
Figure 3.11 The result for the second imaging plates, IP2 from the preliminary fast neutron radiography system

3.3 Experiments on the fast neutron radiography system

Four experiments were carried out with the fast neutron radiography system. An experiment was carried out to verify if the proposed detecting system was competent to be used for fast neutron radiography. Three basic samples were used, i.e., water, paraffin wax and plasticine. The second experiment was to compare the results from three basic samples while the third experiment was to simulate different packaging materials that could probably be used as the packaging for the illicit materials. The last experiment was carried out to test the "unknown" samples that were randomly placed in the tested packaging materials. The results of the experiments were discussed in the following chapter.

The fast radiography system was set up with the system configuration as shown in Figure 3.12. The same experimental setup was maintained for all other experiments. The source to detector distance was 37 cm while the sample was attached to the first imaging plate, IP1. A 2.8 mm acrylic plate was sandwiched between the first imaging plate, IP1 and the second imaging plate, IP2. The identification codes of the samples were placed on top of IP1 while the label "DUP" was used as the identification code for IP2. These identification codes were made from lead. For all the experiments, the imaging plate used as IP1 was always used as IP1 and the same was also applied on IP2.

(a) The experimental setup	(b) The sample and detecting system
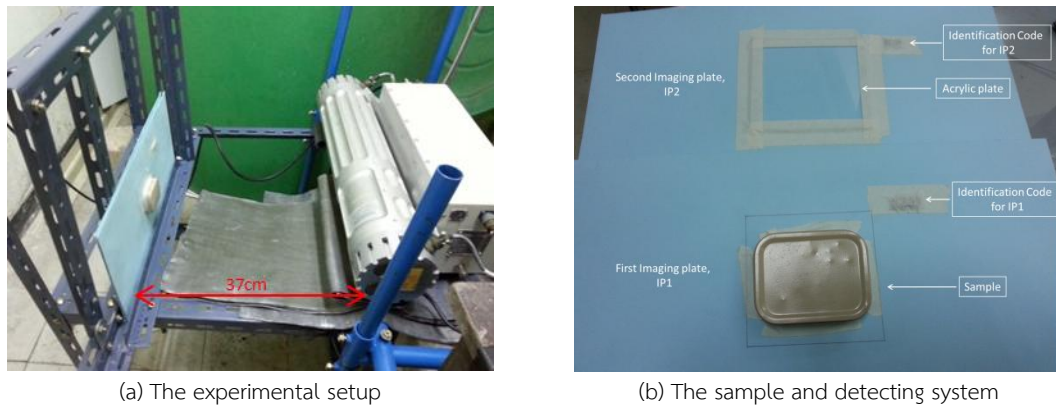
Figure 3.12 The experiment setup and the detecting system for the fast neutron radiography

The same parameters were used for the testing of the other samples. Figure 3.13 showed the user interface of the neutron generator and the arrow in the figure pointed to the parameters that needed to be set. For the neutron generator, the deuteron beam current was set at 60 µA while the high voltage was 75 kV. Each measurement was conducted for 15 minutes and was followed by the reading of the imaging plates. All the imaging plates were read in negative mode, which produced the results similar to that of a film. The reading of two imaging plates took 24 minutes (12 minutes each) and the imaging plates were then put in the imaging plate clearer for at least 15 minutes. Overall, each measurement took approximately 1 hour.
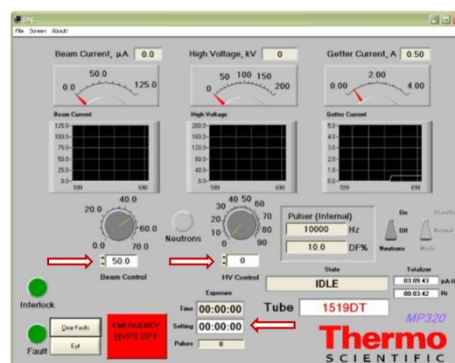
Figure 3.13 The user interface of the neutron generator

The raw images obtained from the "Multi Gauge" software were then exported to a BITMAP file that could be read by "Image J". The position alignment of the image was achieved by adjusting the position of the identification code imprinted by the exposure on both imaging plates. The images were then cropped into the same size to reduce the data size. After that, the "ImageJ" was used to perform the XOR operation on both images.

3.3.1 Testing the proposed detecting system

Three basic samples were used for testing the proposed radiography system, i.e., a packet of water, two pieces of paraffin wax and a piece of plasticine (oil-based modeling clay). These samples were placed in a metal box (dimension: 8.5 cm $\times$ 6.5 cm $\times$ 2.2 cm). In order to differentiate the effect of X-ray and neutrons, the metal screws were put together with the samples. Figure 3.14 showed the samples were put in a metal box.

(a) XN20: Packet of water   (b) XN13: 2 pieces of paraffin wax   (c) XN 14: Piece of plasticine
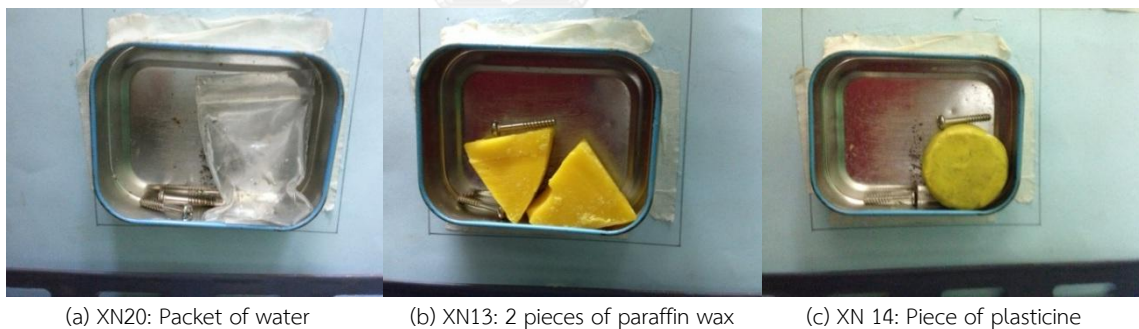
Figure 3.14 The samples used in Experiment 3.3.1

The result images obtained from the first imaging plate, IP1 and the second imaging plate, IP2 were shown in Figure 3.15 and Figure 3.16 respectively. The word "DUP" in the images indicated the result from the second imaging plate, IP2. Figure 3.17 showed the results of XOR operation performed by "ImageJ".

(a) XN20: Packet of water   (b) XN13: 2 pieces of paraffin wax   (c) XN 14: Piece of plasticine

Figure 3.15 The raw images obtained from the first imaging plate, IP1 in

Experiment 3.3.1

(a) XN20: Packet of water   (b) XN13: 2 pieces of paraffin wax   (c) XN 14: Piece of plasticine

Figure 3.16 The raw images obtained from the second imaging plate, IP2 in
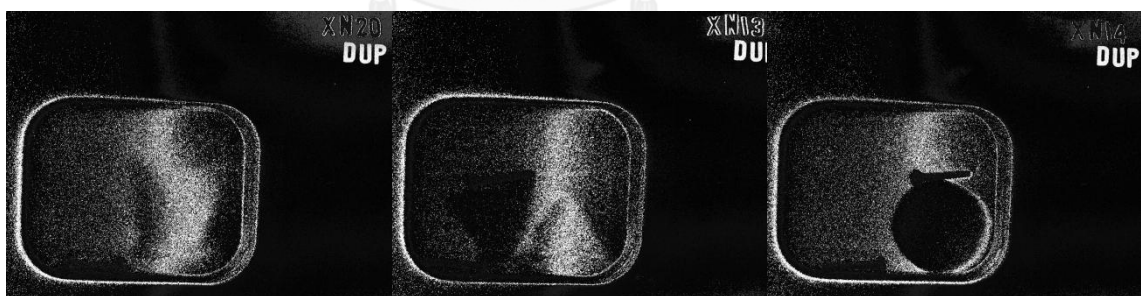
Experiment 3.3.1

(a) XN20: Packet of water   (b) XN13: 2 pieces of paraffin wax   (c) XN 14: Piece of plasticine

Figure 3.17 The results of XOR operation on the images obtained by IP1 and IP2

in Experiment 3.3.1

3.3.2 Comparing three basic samples

The experiment was also set to compare the different samples in the same setting. The different combinations of the water packet, the paraffin wax and the plasticine

placed in the same metal box were used as the sample. Figure 3.18 showed the sample used in experiment 3.3.2.

(a) Paraffin wax and plastcine   (b) Water packet and plasticine   (c) Paraffin wax and water packet

Figure 3.18 The sample used in Experiment 3.3.2

The result images obtained from the first imaging plate, IP1 and the second imaging plate, IP2 were shown in Figure 3.19 and Figure 3.20 respectively. Figure 3.20 showed the result of the XOR operations as performed by "ImageJ".

(a) Paraffin wax and plastcine   (b) Water packet and plasticine   (c) Paraffin wax and water packet

Figure 3.19 The images obtained from the first imaging plate, IP1 in

Experiment 3.3.2

(a) Paraffin wax and plastcine   (b) Water packet and plasticine   (c) Paraffin wax and water packet
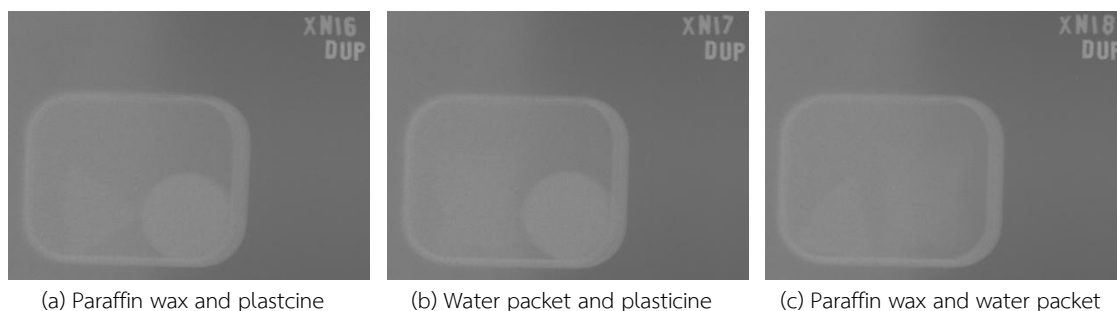
Figure 3.20 The images obtained from the second imaging plate, IP2 in Experiment 3.3.2

(a) Paraffin wax and plastcine   (b) Water packet and plasticine   (c) Paraffin wax and water packet
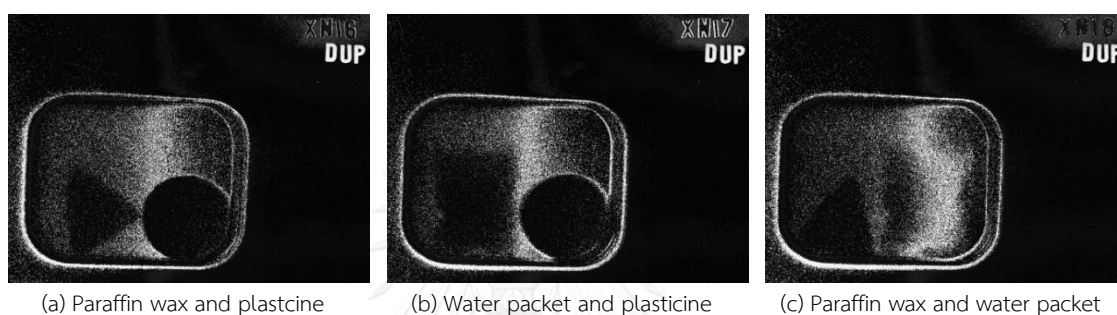
Figure 3.21 The results of XOR operation on the images obtained by IP1 and IP2 in Experiment 3.3.2

3.3.3 Testing the effect of the various packaging materials

In this experiment, four common packaging materials were used to simulate the packaging of the illicit substance. Four of them were a plastic box, a cotton bag, a paper box and a glass container with plastic cover (as shown in Figure 3.22). Three basic samples, i.e., a packet of water, two pieces of paraffin wax and a piece of plasticine, were placed in these packaging materials.

(a) Cotton bag, plastic box and paper box   (b) Glass container with plastic cover
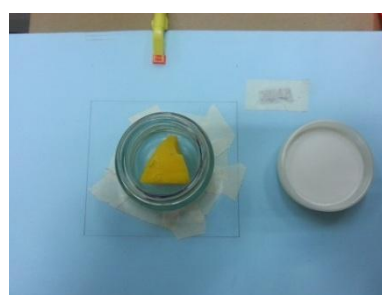
Figure 3.22 The packaging materials used in Experiment 3.3.3

- Results obtained from the plastic box

The result images obtained from the first imaging plate, IP1 and the second imaging plate, IP2 were shown in Figure 3.23 and Figure 3.24 respectively. Figure 3.25 showed the result of the XOR operations performed by "ImageJ".

(a) 2 pieces of paraffin wax   (b) A piece of plasticine   (c) A packet of water
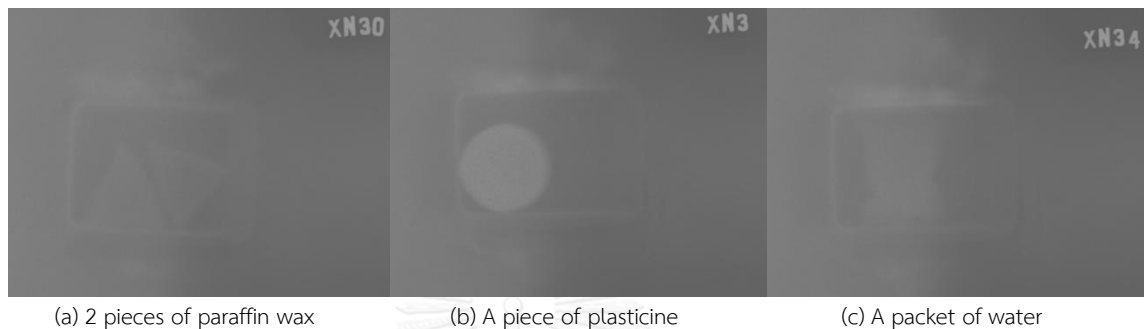
Figure 3.23 The images obtained from the first imaging plate, IP1, for the plastic box used in Experiment 3.3.3

(a) 2 pieces of paraffin wax   (b) A piece of plasticine   (c) A packet of water
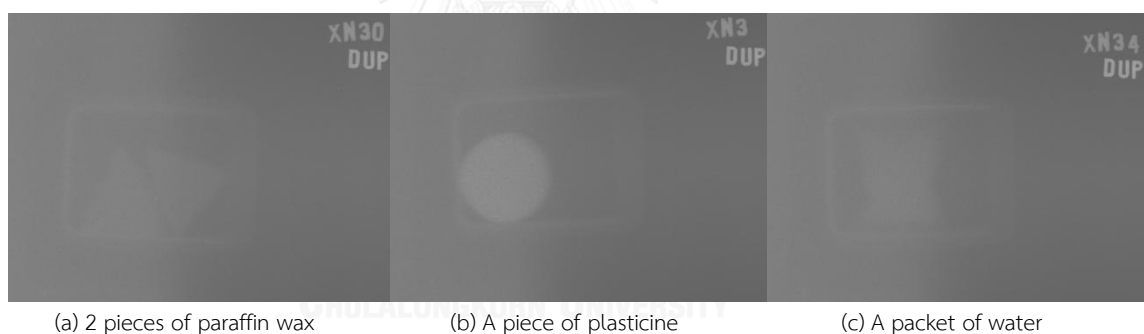
Figure 3.24 The images obtained from the second imaging plate, IP2, for the plastic box used in Experiment 3.3.3

(a) 2 pieces of paraffin wax   (b) A piece of plasticine   (c) A packet of water
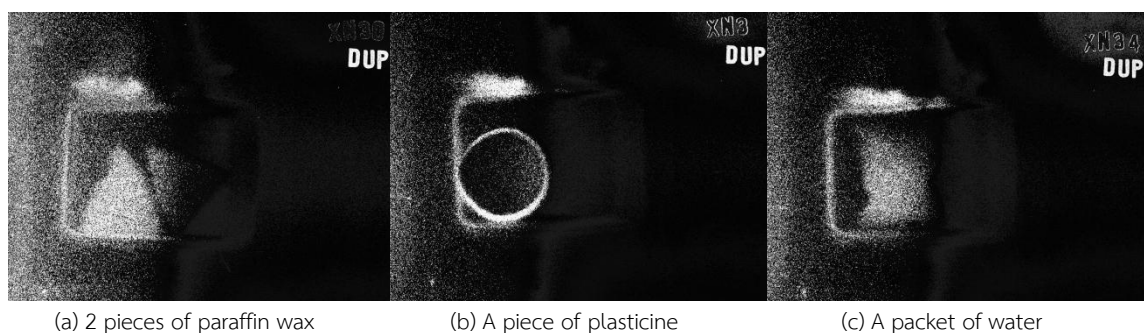
Figure 3.25 The results of XOR operation on the images obtained by IP1 and IP2 for the plastic box used in Experiment 3.3.3

- Results obtained from the cotton bag

The result images obtained from the first imaging plate, IP1 and the second imaging plate, IP2 were shown in Figure 3.26 and Figure 3.27 respectively. Figure 3.28 showed the result of the XOR operations performed by "ImageJ".

(a) 2 pieces of paraffin wax (b) A piece of plasticine (c) A packet of water
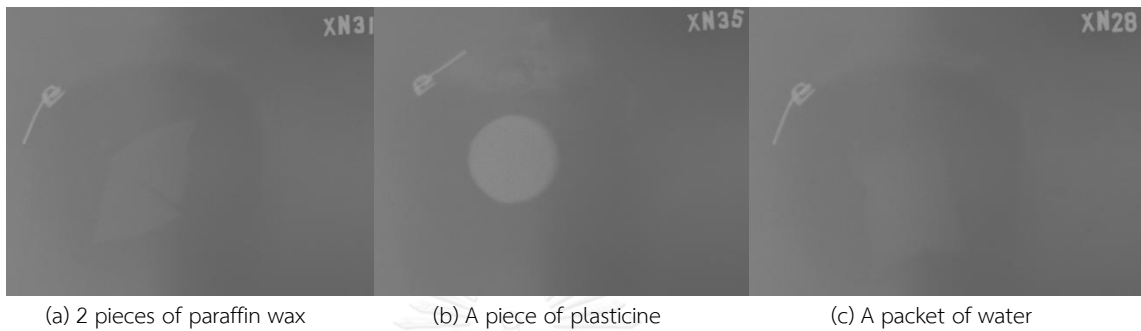
Figure 3.26 The images obtained from the first imaging plate, IP1, for the cotton bag used in Experiment 3.3.3

(a) 2 pieces of paraffin wax (b) A piece of plasticine (c) A packet of water
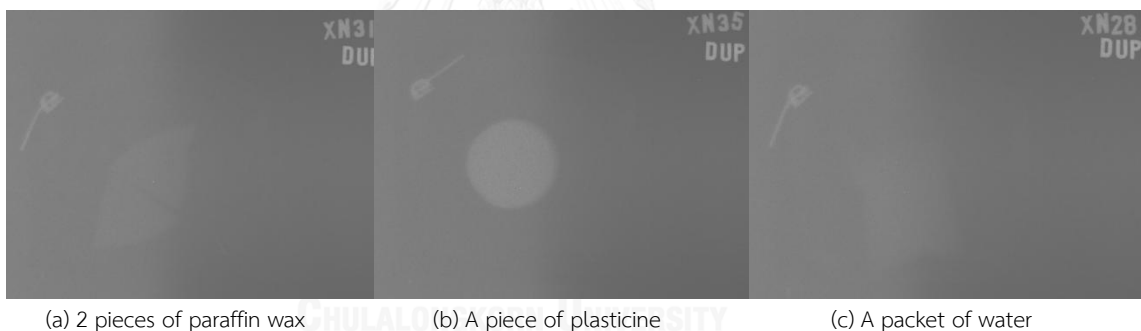
Figure 3.27 The images obtained from the second imaging plate, IP2, for the cotton bag used in Experiment 3.3.3

(a) 2 pieces of paraffin wax (b) A piece of plasticine (c) A packet of water
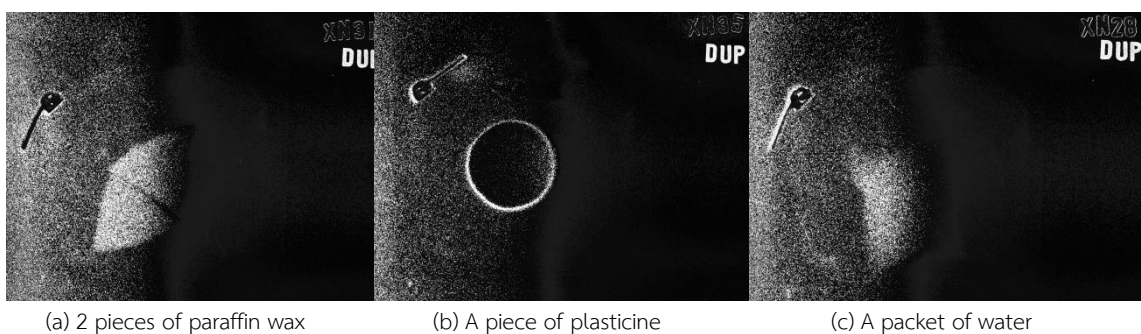
Figure 3.28 The results of the XOR operation on the images obtained by IP1 and IP2 for the cotton bag used in Experiment 3.3.3

- Result obtained from the paper box

The result images obtained from the first imaging plate, IP1 and the second imaging plate, IP2 were shown in Figure 3.29 and Figure 3.30 respectively. Figure 3.31 showed the result of the XOR operations performed by "ImageJ".

(a) 2 pieces of paraffin wax   (b) A piece of plasticine   (c) A packet of water
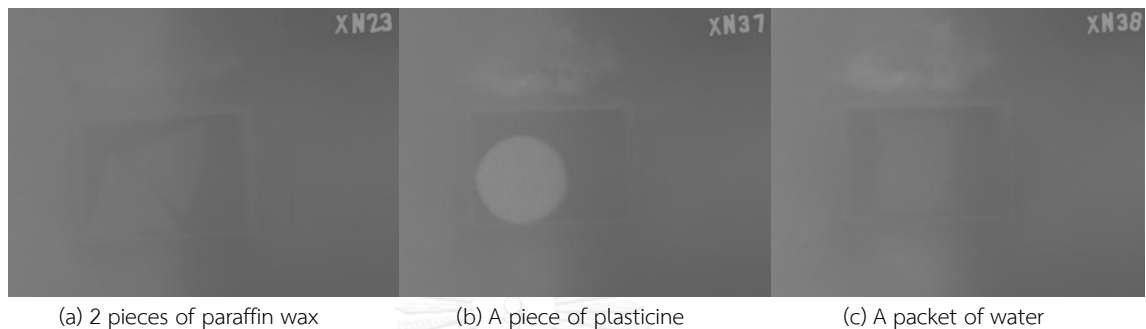
Figure 3.29 The images obtained from the first imaging plate, IP1, for the paper box used in Experiment 3.3.3

(a) 2 pieces of paraffin wax   (b) A piece of plasticine   (c) A packet of water
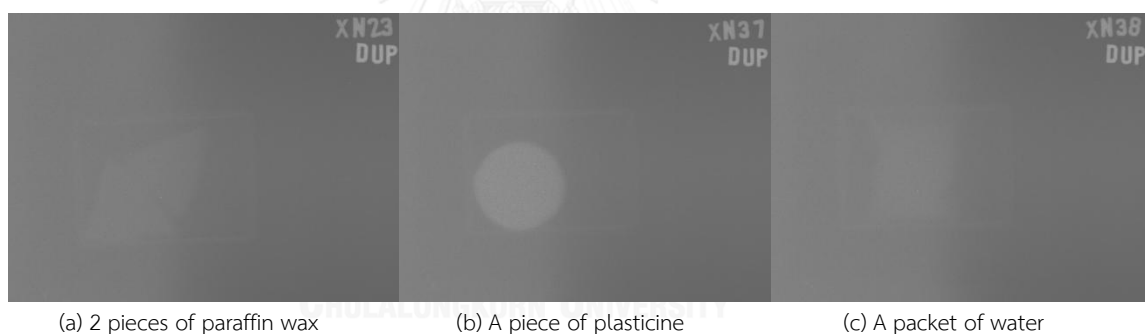
Figure 3.30 The images obtained from the second imaging plate, IP2, for the paper box used in Experiment 3.3.3

(a) 2 pieces of paraffin wax   (b) A piece of plasticine   (c) A packet of water
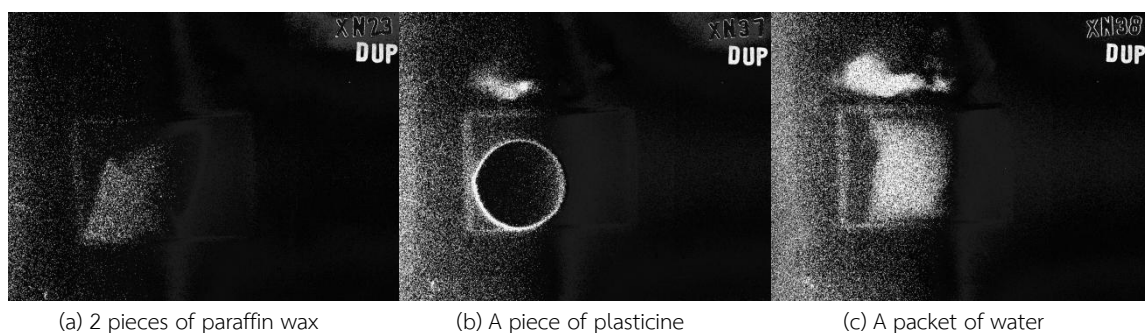
Figure 3.31 The results of XOR operation on the images obtained by IP1 and IP2 for the paper box used in Experiment 3.3.3

● Result obtained from the glass container

The result images obtained from the first imaging plate, IP1 and the second imaging plate, IP2 were shown in Figure 3.32 and Figure 3.33 respectively. Figure 3.34 showed the result of the XOR operations performed by "ImageJ".
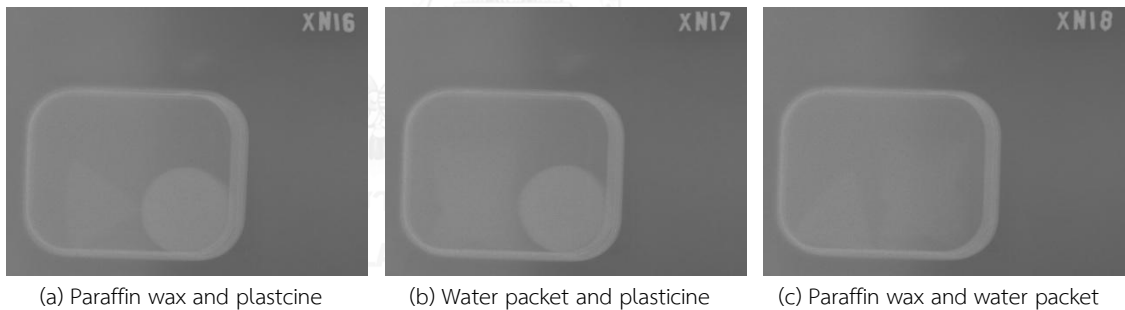

(a) A piece of paraffin wax   (b) A piece of plasticine   (c) A packet of water
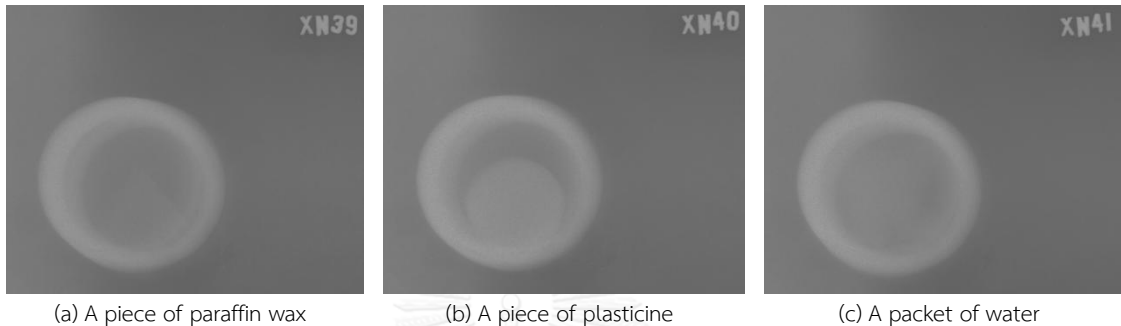
Figure 3.32 The images obtained from the first imaging plate, IP1, for the glass container used in Experiment 3.3.3

(a) A piece of paraffin wax   (b) A piece of plasticine   (c) A packet of water
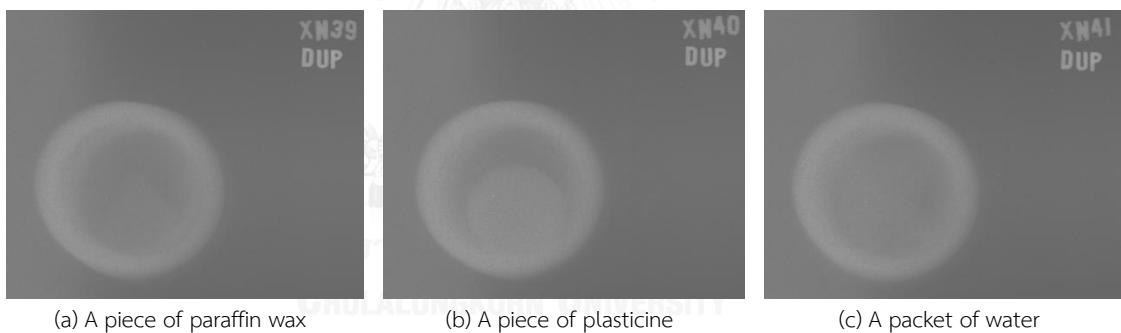
Figure 3.33 The images obtained from the second imaging plate, IP2, for the glass container used in Experiment 3.3.3

(a) A piece of paraffin wax   (b) A piece of plasticine   (c) A packet of water
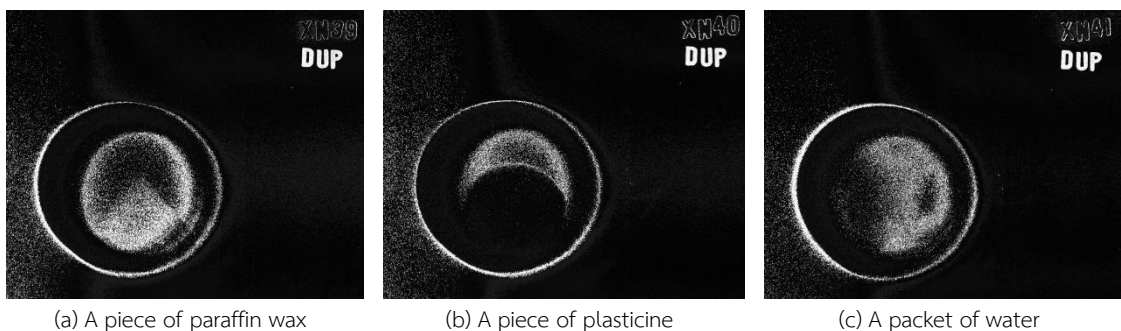
Figure 3.34 The results of XOR operation on the images obtained by IP1 and IP2 for the glass container used in Experiment 3.3.3

3.3.4 Testing the unknown samples

The last experiment was to use the fast neutron radiography system for testing the "unknown" samples. The "unknown" samples used in the system were a piece of chocolate, a packet of gasohol, two tablets of fertilizers, two pieces of *Mochi* (confectionery) filled with the screw nuts and with a small nickel coated plastic ball respectively. These "unknown" samples were placed in two types of packaging materials, i.e., the metal box and one of any light packaging materials. Table 3.3 showed the description of the neutron sample and the packaging material used.

Table 3.3 The "unknown" samples used in Experiment 3.3.4
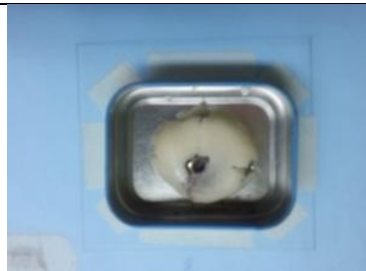
"Unknown" sample	Description	Packaging material (Identification code)	Picture
A piece of chocolate with nut	To demonstrate benign product with the density difference	Metal box (T01), Plastic box (T02)	
A piece of milk chocolate	To demonstrate benign product	Metal box (T03), Paper box (T05)	
A packet of gasohol 95 (10% ethanol)	To demonstrate flammable liquid	Metal box (T04), Paper box (T06)	
Two tablets of fertilizer (14% Nitrogen)	To demonstrate the possible explosive materials	Metal box (T09), Cotton bag (T12)	

Table 3.3 The "unknown" samples used in Experiment 3.3.4 (continued)

"Unknown" sample	Description	Packaging material (Identification code)	Picture
A piece of *Mochi* inserted with nickel coated plastic ball	To test if the system can differentiate among organic materials	Metal box (T07), Plastic box (T10)	
A piece of *Mochi* inserted with screw nuts	To test if the system can differentiate organic materials and metal	Metal box (T08), plastic box (T1)	
Two pieces of gem stones (topaz)	To stimulate benign material or illicit gemstones	Inside and outside Metal box (T13)	

The final XOR results of these samples, according to their identification numbers were shown in Figure 3.35.
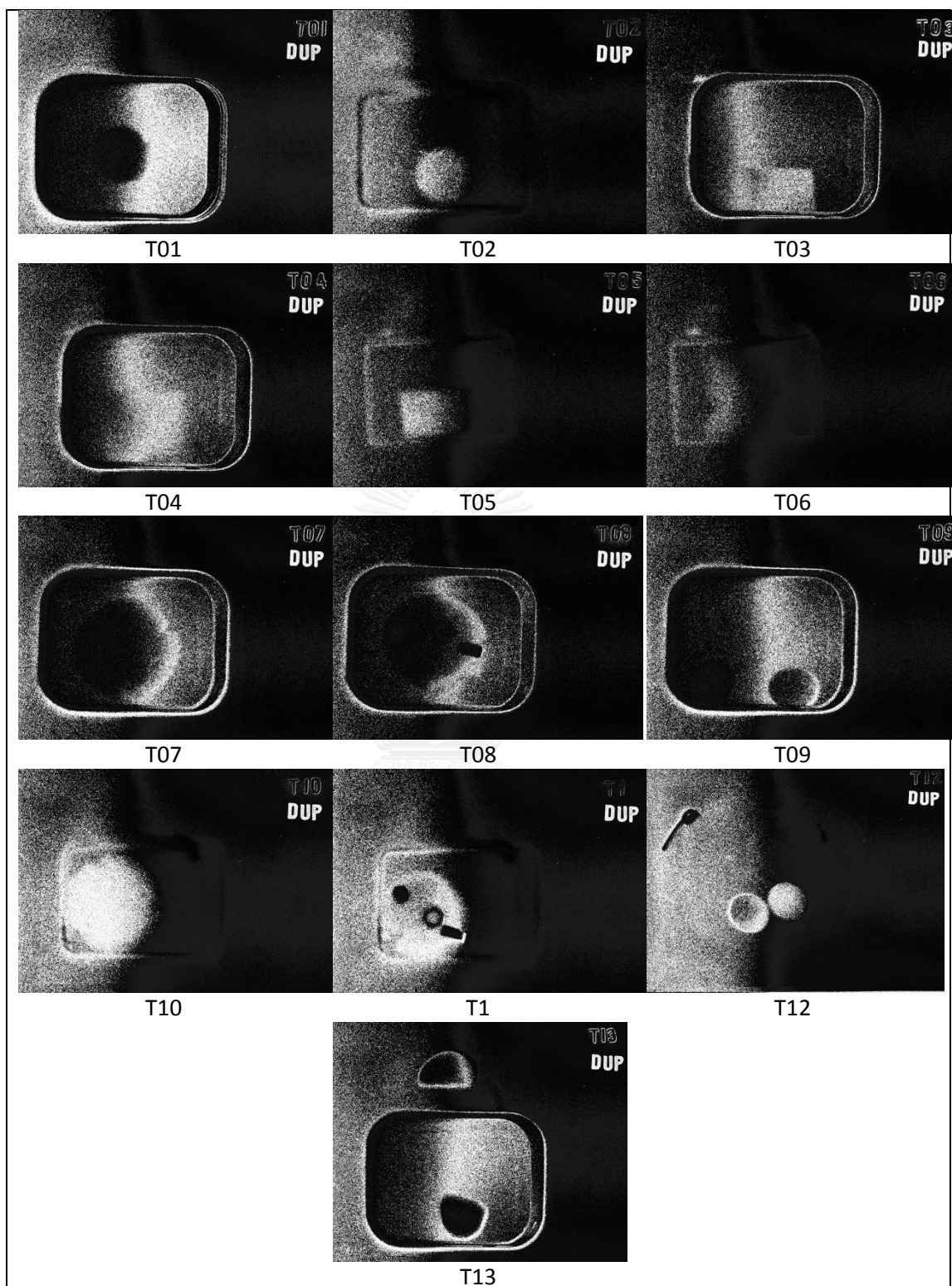
Figure 3.35 The XOR result for the unknown samples tested in Experiment 3.3.4

3.4 Post experiment study: The improvement of image quality

Generally, it was well-known that the image quality could be improved by the adjustment on the brightness and the contrast. The "Microsoft Office 2010" was used to adjust the brightness and the contrast of the cropped raw results. During the adjustment process, the contrast was first being adjusted until the outline of the sample could be better seen. After that the brightness of the image were adjusted to add or reduce the lighting level in the images. In order to see the sample in the images obtained from experiments in Section 3.3, the contrast had to be increased to 100 and the brightness needed to be set as -30. All the raw images obtained were adjusted to the same degree of brightness and contrast. An XOR operation was then again used to produce the resulted images.

Several selected results were shown and discussed in the following chapter. Figure 3.36 showed the raw images, the images after adjusting brightness and contrast, and their XOR operation results respectively.

Sample: XN10: Metal box contains paraffin wax and metal screws
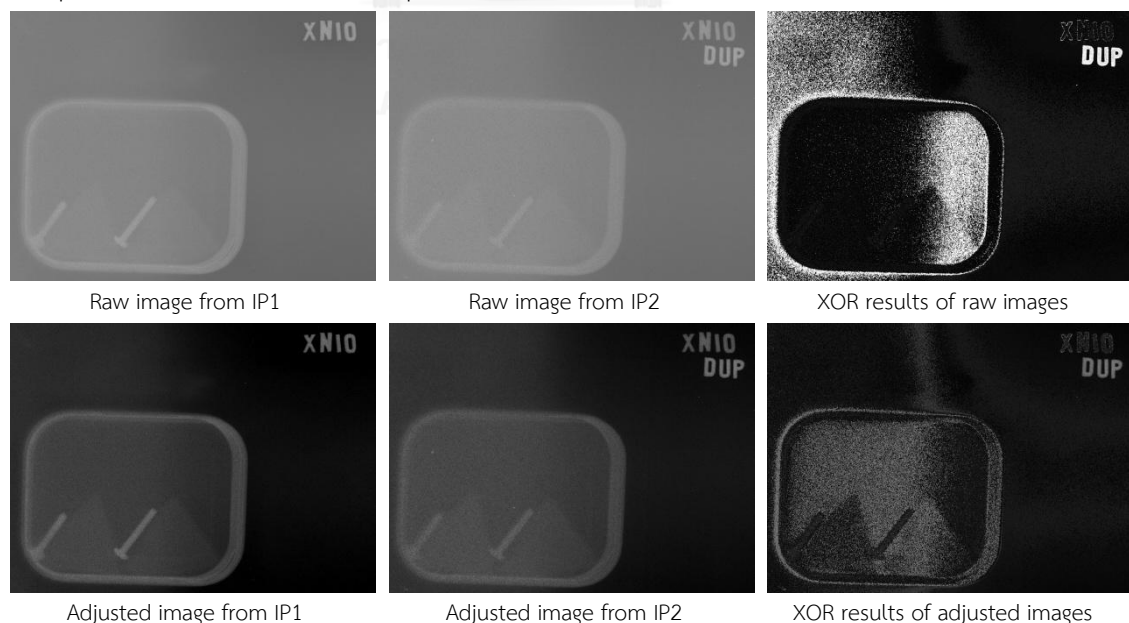
| Raw image from IP1 | Raw image from IP2 | XOR results of raw images |
| Adjusted image from IP1 | Adjusted image from IP2 | XOR results of adjusted images |

Figure 3.36 The raw images, the images after adjusting the brightness and the contrast, and their XOR operation results

Sample: XN28: Cotton bag contains water packet

| Raw image from IP1 | Raw image from IP2 | XOR results of raw images |

| Adjusted image from IP1 | Adjusted image from IP2 | XOR results of adjusted images |
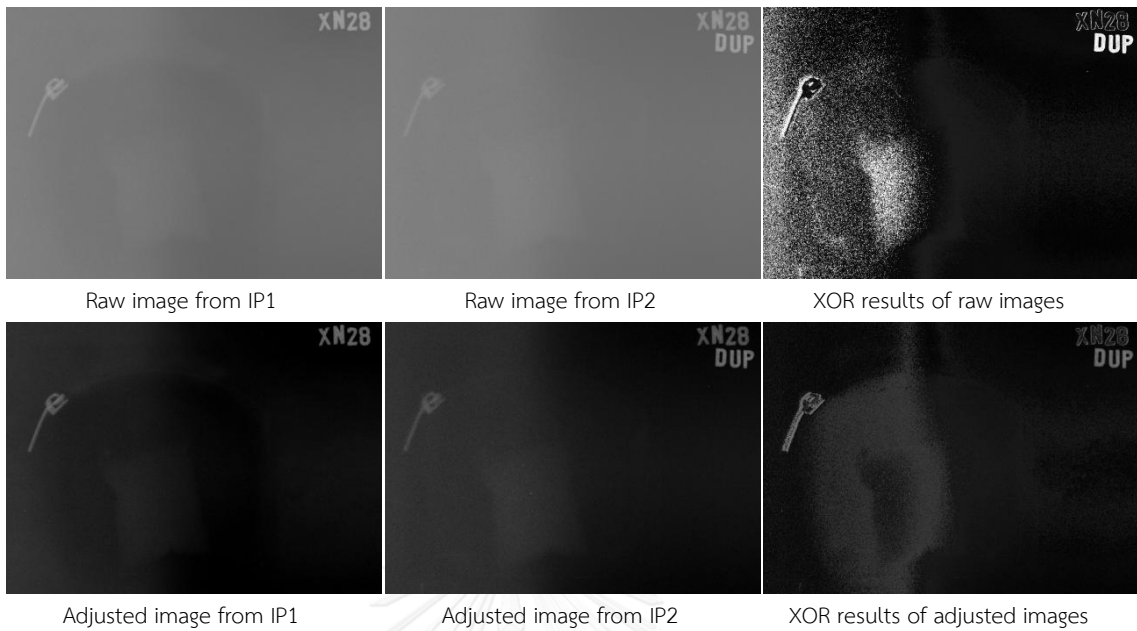
Sample: T09: Metal box contains two tablets of fertilizers
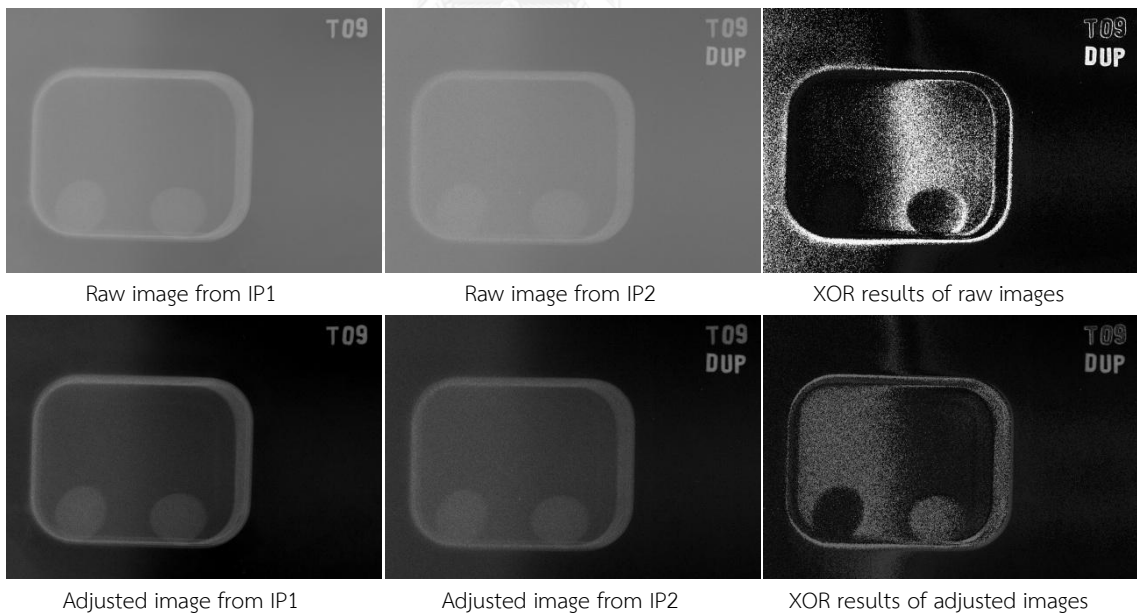
| Raw image from IP1 | Raw image from IP2 | XOR results of raw images |

| Adjusted image from IP1 | Adjusted image from IP2 | XOR results of adjusted images |

Figure 3.36 The raw images, the images after adjusting the brightness and the contrast, and their XOR operation results (continued)

Sample: XN32: Paper box contains two pieces of paraffin wax

| Raw image from IP1 | Raw image from IP2 | XOR results of raw images |

| Adjusted image from IP1 | Adjusted image from IP2 | XOR results of adjusted images |
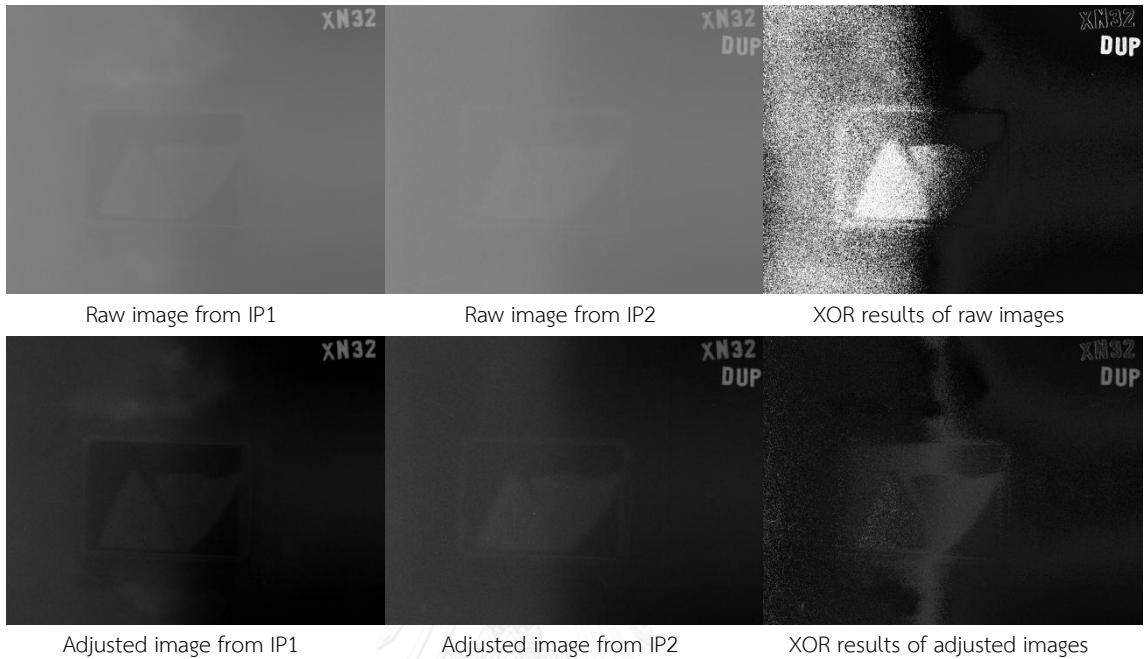
Sample: T04: Paper box contains *Mochi* inserted metal screw nut
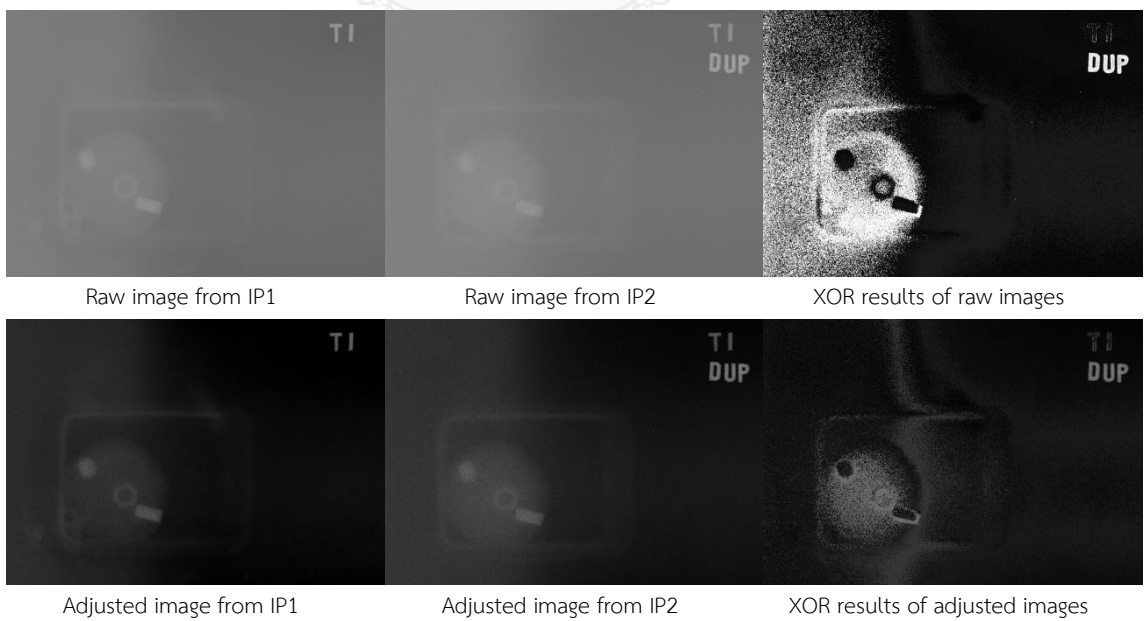
| Raw image from IP1 | Raw image from IP2 | XOR results of raw images |

| Adjusted image from IP1 | Adjusted image from IP2 | XOR results of adjusted images |

Figure 3.36 The raw images, the images after adjusting the brightness and the contrast, and their XOR operation results (continued)

CHAPTER 4

RESULT ANALYSES AND DISCUSSIONS

Based on the results described in Chapter 3, the images from the fast neutron radiography were analyzed and discussed. The discussion began from the experiments on the fast neutron radiography system (Section 3.3) and followed by the image quality improvement by adjusting brightness and contrast (Section 3.4).

4.1 Analysis on the experiments on the fast neutron radiography system

There were four experiments carried out in Section 3.3. The first on was to test the proposed detecting system. The samples used were a metal box containing three basic samples that were supposedly sensitive with the neutrons and the metal screw that was sensitive with the X-ray. The second experiment was to compare the three basic samples while the third one was to study the effect of the various packaging materials. The last experiment was to test the system with the "unknown" samples.

4.1.1 Analysis on the testing of the proposed detecting system

In this section, the discussion is based on the results in part 3.3.1.

Figure 3.15 showed the raw results from the imaging plate, IP 1 without any adjustment of the brightness and the contrast. With the existence of the X-ray, the screws, the identification code and the metal box could be clearly observed in the images obtained. In comparison, among three samples, the water packet was most difficult to be identified. The triangle-shaped paraffin wax was shown with the low contrast against the background while the round-shaped plasticine could be easily observed.

Figure 3.16 showed the raw results from the imaging plate, IP2. In general, the information obtained in the second imaging plate, IP2, was similar to that of the first imaging plate, IP1. However, the contrast and the sharpness of the image with the background were relatively poor compared with IP1, especially for paraffin wax (Figure 3.16 (b)). These phenomena could perhaps due to the acrylic plate that was used as the shielding material. Since the acrylic plate could interact with the fast neutrons and caused them to become diffusive, the result would be less clear and even blurred at the edge. The reduction in the sharpness could probably be the result of the increase in the detector to sample distance due to the additional thickness of the shielding materials.

The results of the XOR operation were shown in Figure 3.17. Based on the results, we found that the pixel was in white color if the inputs contained the different information and in black color if the information was the same for both inputs. Since the words "DUP" appeared only on the image from IP2 but not IP1, the result of combining two images clearly showed the words "DUP" in white color. Inversely, the background areas of both image plates shared the similar information (no information), so the result showed the black color for the background.

In comparison to the images before the processing, the contrast in the original image obtained from the imaging plates was enhanced by the XOR operations. As the results, the shapes of the water packet, the paraffin pieces and the plasticine were clearly identified. On the contrary, the screws became less identifiable and merged into the background. The edges of the metal box and identification in all three images were in white color. This might be caused by the imperfect alignment of the images or the shadow appeared in IP2.

Based on the results obtained, the sharpness of the sample could be used to differentiate the metal and organic materials. The metal which was very sensitive to the X-ray would tend to show their edge sharply while the sharpness for the neutron

sensitive materials was less. This could be maintained after the XOR operation if the position alignment was perfect.

The raw image obtained from IP1 and IP2 were significantly affected by X-ray. However, with the XOR operation, the neutron information could be obtained. It was reflected that the acrylic plated used was able to shield up a fraction of incoming fast neutron. The attenuation factor, (Ix/Io) of the acrylic plate was calculated as following.
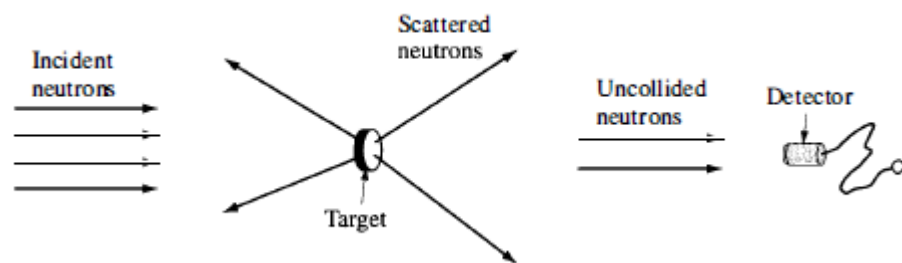
Figure 4.1 Measurement of neutrons that have not collided in a target [34]

With the consideration that the incident neutrons was I(o) and the uncollided neutrons was I(x). I(x) could be calculated as in the following equation [34].

$$I(x) = I(o)e^{-\Sigma_t x}$$

where Σ_t was the total macroscopic cross section of the target and x was its thickness.

$$\Sigma_t = \sigma_t N$$

For the compound consisting of more than one element, the Σ_t could be calculated as follow [35];

$$\Sigma_t = \sigma_{ti} N_i$$

where N was the atomic density and could calculated as follow;

$$N_i = \frac{\rho N_a n_i}{M}$$

where ρ was density of the compound; N_a was the Avogadro's number; M was the molecular weight of the compound; and n_i was the number of atoms of element *i* in one molecule.

For the acrylic shield, the monomer of acrylic was $C_2H_5O_8$. The density of the acrylic was $1.18g/cm^3$ while the molecular weight was 157 (2×12 + 5×1 + 8×16). The total microscopic cross section, σ_t at I4.1 MeV fast neutron for H, C, and O, was as shown in Table 4.1.

Table 4.1 The microscopic cross section, σ_t for I4.1 MeV fast neutron of H, C and O

Element	σ_t at 14.1MeV (barn) [36]
H (H-1)	0.6827954
C (C-12)	1.3205526
O (O-16)	1.5936967

The macroscopic cross section of acrylic was then equal to

$$\Sigma_t = \frac{\rho \times N_a}{M} (\sigma_C n_C + \sigma_H n_H + \sigma_O n_O)$$

$$\Sigma_t = \frac{1.18 \times 6.022 \times 10^{23}}{157 \times 10^{-24}} (1.3205526 \times 2 + 0.6827954 \times 5 + 1.5936967 \times 8)$$

$$\Sigma_t = 0.0851 cm^{-1}$$

I(x) that reached the IP2 was calculated as

$$I(x) = I(o)e^{-\,0.0851cm^{-1}(0.28cm)}$$

$$I(x) = 0.976\,I(o)$$

It meant the acrylic plate attenuated 2.4% of incoming 14.1 MeV fast neutrons.

4.1.2 Analysis on the testing of three basic samples

Just like the raw results in the previous section, the plasticine could be clearly seen among three samples. The shape of the paraffin wax could also be recognized. Among all three, the contrast for the water packet was the worst. Since the plasticine might contain some heavy elements, it could interact better with the X-ray. Relatively, the attenuation of the X-ray by the paraffin wax and the water packet was less significant.

All the samples could be identified after the XOR operations. The contrast for the case of the water packet and paraffin wax samples were significantly improved. It reflected that they could interact with the neutrons better as they were made up of only the light elements, i.e., hydrogen, carbon and oxygen. In comparison, the paraffin wax was able to block the neutron better due to its rich content of hydrogen and carbon. The total macroscopic cross section, Σ_t for 14.1 MeV fast neutrons of these two materials were calculated and compared (shown in Table 4.2).

Table 4.2 The properties and the total macroscopic cross section, Σ_t for 14.1 MeV fast neutron of paraffin wax and water

Material	Paraffin Wax	Water
Molecular Formula	$C_{31}H_{64}$	H_2O
Density, ρ	0.9 g/cm^3	1.0 g/cm^3
Molecular weight, M	436	18
Calculated Σ_t	0.1052 cm^{-1}	0.09897 cm^{-1}
Calculation of Ix/Io if x=1cm	$I(x) = I(o)e^{-0.1052cm^{-1}(1cm)}$ $I(x)/I(o) = 0.9001$	$I(x) = I(o)e^{-0.09897cm^{-1}(1cm)}$ $I(x)/I(o) = 0.9057$

The thickness of the sample could be also one of the factors of fast neutron radiography. Since the water was packed in a plastic bag, the thickness at the edge was less compared with the middle part. This could be one of the reasons why the edges of water packet were more difficult to be identified.

4.1.3 Analysis on the testing of the effect of various packaging materials

As mentioned before, the cotton bag, the plastic box, the paper box and the glass container were used as the packaging materials for the plasticine, the water packet and the paraffin wax samples. Basically, the packaging materials could be divided to two groups; the dense and sold material, i.e., glass and the light materials group, which included the plastic, the paper and the cotton.

In comparison among the light packaging materials and the metal box, the contrast between the samples and its background for the light packaging materials was better than that of metal box; especially for the first imaging plates (refer to Figure 3.23, Figure 3.26 and Figure 3.29). The reason was that the background surrounding the sample was darker than that of the other background part in the

images. This could be clearly observed on the image of the cotton bag (Figure 3.26). Since more radiation exposure caused the image to be darker, this additional radiation was probably contributed by the hydrogen content in the packaging materials. In such case, when a fast neutron collided with a hydrogen nucleus, the proton would be rejected. This recoiled proton could easily penetrate the thin packaging materials and be detected by the imaging plate.

Similar to the previous cases which used a metal box as a packaging material of the sample, the image obtained from the second imaging plate, IP2 of the light packaging materials provided the similar information as the first imaging plate, IP1. The level of the contrast in the image of IP2 was less than that of IP1, especially the samples placed in the paper box (refer to Figure 3.30). Since the recoiled proton produced from the packaging materials could not easily reach IP2, the contrast of IP2 was less distinct than that of IP1.

Based on the XOR operation results obtained light materials group (refer to Figure 3.25, Figure 3.28 and Figure 3.31), the plasticine sample could be easily identified in the all packaging materials but some parts of the water packets and the paraffin waxes were not shown in the resulted images. This might due to the fast neutron attenuation efficiency of the water packets and the paraffin waxes were similar with that of the light packaging materials as their atomic composition and the density might similar.

For the glass container, based on the raw images obtained from IP1 and IP2 (Figure 3.32 and Figure 3.33), the water package could not be identified while the paraffin wax piece could be observed with low contrast. The information in the raw images obtained from the glass container was similar with that of the metal box. As shown in Figure 3.34, the XOR operation clearly showed the paraffin wax piece but the plasticine was observed to blend with the background which was that of the container. This reflected that the neutron interactions with the plasticine and with the glass were about the same effectiveness. Both of them might contain some

elements that were not sensitive to neutrons. On the other hand, the water packet was harder to identify although part of it could be observed. This might be due to the distortion of its shape when it was put in a tight container.

4.1.4 Analysis on the testing of the unknown samples

In this section, the image analyses were done based on the XOR operation results shown in Figure 3.35. From the results obtained, the packaging materials could be clearly identified; the one with the very good sharpness were the images obtained from the metal box (T01, T03, T04, T07, T08, T09 and T13), while the less clear rectangular shapes (T02, T05, T06, T10 and T1) were obtained from either the plastic box or the paper box. T12, which did not show the shape of packaging material but showed the image of the metal zip was actually from the case with the cotton bag.

With the same samples, the images obtained for the cases with metal box and with the light packaging materials showed the same outline but the grayness of the images were different. Except the over exposure at the right part of images, the light materials packaging provided the images that were easier to identify compared with that from the metal box. The sharpness and the contrast of the unknown samples were also not as good for the case of the metal box.

The results of the chocolate with and without the nut inside were similar (T01 and T02 for chocolate with nut while T03 and T05 for the chocolate without nut). The fast neutron radiography also could not differentiate the nickel coated plastic ball from the *mochi* (T07 and T10). On the other hand, the metal screw nuts could be clearly observed and differentiated (T08 and T1), especially the one placed in the plastic box (T1). The reason for this behavior was perhaps because the nickel that coated the plastic ball was too thin to have any effect.

For the unknown samples that simulated the possible explosive, the fertilizers could be clearly identified (T09 and T12), especially the one placed in the

cotton bag (T12). On the other hand, the gasohol could be identified only after the XOR operations with a low contrast and sharpness (T04 and T06). This might be the result from its low density and irregular shape.

The last samples of this experiment were the gem stones placed inside and outside the metal box (T13). The information obtained with and without the packaging materials was the same. From the sharpness of the samples, it was suggested that the fast neutron had about the same effect on this samples as that of the plasticine.

4.2 Analysis on the post experiment study

One of the advantages of using the imaging plates was that the images could be stored digitally. Hence, the improvement of image quality was much easier compared with the uses of the film. In this study, only the basic adjustment functions for the digital images were applied, i.e., the adjustment of the contrast and the brightness. The discussion in this section was based on the images as displayed in Figure 3.36.

The sharpness of the images was significantly improved after adjusting the contrast and the brightness. Referring to XN10 and XN 28, the pieces of paraffin and the water packet could be easier identified comparing with the results before the adjustment. The adjustment of the brightness and the contrast also enhanced the difference between the samples and the background, i.e., the background became darker after the adjustment.

The XOR operation results from the adjusted images were quite different from the results from the raw input. For the adjusted images, the word "DUP" was still shown up in the images, however the color was grey which indicated the difference between two inputs were smaller comparing with the difference found in the raw inputs. Due to the decrease of the brightness, the grey value in pixels of the

adjusted images was decreased. The word "DUP" had the relatively darker tone than that of raw images. Therefore the difference calculated by the XOR operation showed a smaller difference and made the tone darker.

Based on the images shown in Figure 3.36, some of the XOR operations results were significantly improved with the adjustment on the brightness and the contrast. The sample XN10, where the metal box contained the paraffin wax and the metal screws, was a good example of this adjustment. The XOR results for the raw inputs could not differentiate the paraffin wax from the background. This was significantly improved by the adjustment on the brightness and the contrast for the raw images. The same pattern was observed for the sample XN28, where the cotton bag contained the water packet, and sample T09, where the metal box contained two tablets of fertilizers. Especially for T09, only one tablet of fertilizer could be seen in the XOR result on the raw images. After adjusting the brightness and the contrast, both tablets could then be observed.

However, not all images were significantly improved with the adjustment on the brightness and the contrast. For example, the sample XN32, where the paper box contained two pieces of paraffin wax, the pieces of paraffin wax could be observed in the XOR results of the raw image even though the raw input of IP1 and IP2 could not show the paraffin wax clearly. However, the XOR operation on the adjusted images made it harder to observe the edge of paraffin waxes due to the low contrast against background. The same situation also happened to the unknown sample T04. All three metal screw nuts could be observed in the XOR result of the raw images. For the XOR result of the adjusted images, one of the screw nuts located at the center of the *mochi* could not be identified but the edge of the *mochi* was clearer. Generally, it was concluded that the adjustment of the brightness and the contrast of the raw images could improve the sharpness of the XOR results but not their contrast.

CHAPTER 5

CONCLUSION

In this chapter, all the works were summarized and concluded. At the end of this chapter, several suggestions were given for those researchers who might be interested with this work.

5.1 Summary

A fast neutron radiography system based on a 14.1 MeV portable neutron generator was proposed and studied. As the neutron generator emitted a significant intensity of X-ray, the study was aimed to develop the basic configuration for fast neutron radiography system which could provide an image of sufficient information in which the effect for the X-ray was reduced. In this work, the detecting system used was two identical imaging plates with an acrylic plate inserted in between to attenuate the fast neutron. As both the imaging plates shared the same information of X-ray but different information for fast neutron, a binary operation, XOR operation was then proposed to extract the difference caused by the fast neutron in two imaging plates.

The profile of the neutron generator was studied by adjusting its beam current and high voltage and there was no significant difference between the neutron yield and the X-ray yield observed. Therefore, the parameters of the neutron generators chosen were at a level of beam current which could produce a sufficient amount of deuterons and a high enough values of high voltage which could accelerate the deuterons to the tritium target plate.

Another preliminary study was to test the applicability of a lead sheet to be used as the shielding materials. The results showed that the lead sheet could attenuate most of the X-ray before reaching to the second imaging plates. It was

then considered that the lead sheet would not be suitable to be used as the shielding material.

The first experiment was to test the proposed fast neutron system. The results found that the proposed system could effectively reduce the effect of X-ray and the light element could be detected. The second experiment was to compare the three basic samples. The results found that the light elements which had similar effectiveness on shielding the fast neutrons would have the similar image quality. Some of the heavy elements would provide less quality image after XOR operation.

The third experiment was to test the effect of various packaging materials. The results found that the samples could be more difficult to be detected if the packaging materials were about the similar density and atomic composition to the samples. The images would blend together if the samples and the packaging materials had the similar effectiveness on attenuating the fast neutrons.

The last experiment was to test the unknown samples by the fast neutron system. The results showed that the system could detect both the metal and organic material. The sharpness of images could be used to differentiate the metals and organic materials. The sharpness of the metals was better than that of organic materials.

The images quality could be improved by adjusting the brightness and the contrast of the raw results from the imaging plates. After adjustment, the contrast and the sharpness of the images were improved and the samples could be easier identified. Generally, the adjustment of the brightness and the contrast could improve the sharpness of the XOR results but not their contrast.

Overall, it was concluded that the proposed fast neutron radiography system could provide an image with sufficient information in which the X-ray effect was

reduced. The metals and the organic materials could be differentiated by the system. Hence, the objective of the study was achieved.

5.2 Suggestions

It was suggested to study the profile of the X-ray and the neutrons produced by the neutron generator prior to the designing of the fast neutron radiography system. As experienced in this study, the difference in radiation intensity affected the image quality of results. Therefore, some of the problems could be avoided.

The second suggestion was to normalize the grey value before the XOR operations. As the detection efficiency of the imaging plates could be varied from one to another even when their specifications are the same. By using the normalized value, the intrinsic difference between two imaging plates could be diminished and thus provided a better XOR result.

As the neutron intensity of the portable neutron generators was low, the (n, 2n) and (n, 3n) reactions could be utilized to increase the neutron intensity. With a high intensity of neutrons, a collimator could then be used to obtain the better raw images.

The X-ray sensitive imaging plates could also be applied in the fast neutron radiography system due to the presence of the recoiled protons. In order to obtain the fast neutron information, the imaging plates should not be overexposed. Otherwise the XOR results would have become saturated.

REFERENCES

[1]   National Consortium for the Study of Terrorism and Responses to Terrorism (START). **Global Terrorism Database** [Online]. 2013. Available from: http://www.start.umd.edu/gtd [10th October, 2014]

[2]   Andy Buffler. Contraband detection with fast neutrons. **Radiation Physics and Chemistry** 71 (2004) : 853–861.

[3]   Richard C. Lanza. Neutron Techniques for Detection of Explosives. In Jehuda Yinon, **Counterterrorist Detection Techniques of Explosives**, 131-155. Amsterdam : Elsevier B.V., 2007.

[4]   B.D. Sowerby and J.R. Tickner. Recent advances in fast neutron radiography for cargo inspection. **Nuclear Instruments and Methods in Physics Research A** 580 (2007) : 799–802.

[5]   J.E. Eberhardt, S. Rainey, R.J. Stevens, B.D. Sowerby, J.R. Tickner. Fast neutron radiography scanner for the detection of contraband in air cargo containers. **Applied Radiation and Isotopes** 63 (2005) : 179–188.

[6]   Y. Liu, B.D. Sowerby, J.R. Tickner. Comparison of neutron and high-energy X-ray dual-beam radiography for air cargo inspection. **Applied Radiation and Isotopes** 66 (2008) : 463–473.

[7]   Nares Chankow. Neutron Radiography. In Dr. Mohammad Omar, **Nondestructive Testing Methods and New Applications**, 73-100. Rijeka : InTech, 2012.

[8]   J.G. Fantidis, G.E.Nicolaou, N.F.Tsagas. Optimization study of a transportable neutron radiography unit based on a compact neutron generator. **Nuclear Instruments and Methods in Physics Research A** 618 (2010) : 331–335.

[9]   V.D. Aleksandrov, E.P. Bogolubov, O.V. Bochkarev,L.A. Korytko, V.I. Nazarov, Yu.G. Polkanov, V.I. Ryzhkov, T.O. Khasaev. Application of neutron generators for high explosives, toxic agents and fissile material detection. **Applied Radiation and Isotopes** 63 (2005) : 537–543.

[10]   Wu Yang, Tang Bin, Huo Heyong, Liu Bin, Tang Ke, Sun Yong, Yin Wei, Cao Chao. The study of zinc sulphide scintillator for fast neutron radiography. **Physics Procedia** 43 (2013) : 205 – 215.

[11]   Gad Shani. Fast Neutron Radiography system. **United States Patent** 4535246 (13 Aug, 1985).

[12]   Jacob G Fantidis, Bandekas V Dimitrios, Potolias Constantinos and Vordos Nick. Fast and thermal neutron radiographies based on a compact neutron generator. **Journal of Theoretical and Applied Physics** 6 (September 2012).

[13]   Erzsebet Svab and Marton Balasko. Non-destructive Testing: Neutron Radiography. In Yuri M. Tsipenyukaytexa, **Physical Methods, Instruments and Measurements Volume IV**, 203-231. Encyclopedia of Life Support Systems (EOLSS), 2008.

[14]   V.O. de Haan, T.H.J.J. van der Hagen, A. Fedorov, A. van Veen, P.F.A. de Leege. Conceptual design of a novel high-frame-rate fast-neutron radiography facility. **Nuclear Instruments and Methods in Physics Research A** 539 (2005) : 321–334.

[15]   Hang Li, Yubin Zou, Sheng Wang, Weiwei Wen, Shuquan Liu, Guoyou Tang, Yuanrong Lu, Zhiyu Guo. Preliminary experiments of neutron radiography with several hunderd keV fast neutrons. **Physics Procedia** 43 (2013) : 66 – 72.

[16]   R.M. Ambrosi and J.I.W. Watterson. The effect of the imaging geometry and the impact of neutron scatter on the detection of small features in accelerator-based fast neutron radiography. **Nuclear Instruments and Methods in Physics Research A** 524 (2004) : 340-354.

[17]   J. Reijonen, N. Andresen, F. Gicquel, R. Gough, M. King et. al. Development of advanced neutron/gamma generators for imaging and active interrogation applications. **Proc. SPIE** 6540 (May 2007).

[18]   Shigenori Fujine, Kenji Yoneda, Koji Yoshii, Masahiro Kamata, Masayoshi Tamaki, Kohei Ohkubo, Yasushi Ikeda, Hisao Kobayashi.   Development of imaging techniques for fast neutron radiography in Japan.   **Nuclear Instruments and Methods in Physics Research A** 424 (1999) : 190-199.

[19]   Toshiya Sanami, Mamoru Baba, Keiichiro Saito, Tetsuro Yamazaki, Takako Miura, Yasutaka Ibara, Shingo Taniguchi, Akira Yamadera,Takashi Nakamura. Fast-neutron profiling with an imaging plate.   **Nuclear Instruments and Methods in Physics Research A** 458 (2001) : 720-728.

[20]   Masahito Matsubayashi, Takashi Hibiki, Kaichiro Mishima, Koji Yoshii, Koji Okamoto.   Preliminary examination of the applicability of imaging plates to fast neutron radiography.   **Nuclear Instruments and Methods in Physics Research A** 463 (2001) : 324–330.

[21]   V. Mikerov, V. Samosyuk, S. Verushkin.   Detectors based on imaging plates for fast neutron radiography.   **Nuclear Instruments and Methods in Physics Research A** 542 (2005) : 192–196.

[22]   Nares Chankow, Suvit Punnachaiya, Sarinrat Wonglee.   Neutron radiography using neutron imaging plate.   **Applied Radiation and Isotopes** 68 (2010) : 662-664.

[23]   IAEA.   **Neutron Generators for Analytical Purposes**.   Radiation Technology Reports Series No. 1.   Vienna: International Atomic Energy Agency, 2012.

[24]   Thermo Scientific.   **Product Specification of Thermo Scientific MP320 Lightweight, Portable Neutron Generators**.   Colorado : Thermo Fisher Scientific   Inc,   (n.d.).   Available   from: https://static.thermoscientific.com/images/D10497~.pdf [10th April 2014]

[25]   Kenji Takahashla, Seiji Tazaki, Junji Miyahara, Yuuko Karasawa, Nobuo Niimura. Imaging performance of imaging plate neutron detectors.   **Nuclear Instruments and Methods in Physics Research A** 377 (1996) : 119-122.

[26]   Pacella D. Energy-resolved X-ray detectors: the future of diagnostic imaging. **Dove Medical Press** 19 January 2015 : 1-13.

[27]   Guohai Wei, Songbai Han, Hongli Wang, Linfeng He, Yu Wang, Meimei Wu, Yuntao Liu, Dongfeng Chen. Experience of the Indirect Neutron Radiography Method Based on the X-ray Imaging Plate at CARR. **Physics Procedia** 69 (2015) : 258 -264.

[28]   M. Thoms, D. Myles, C. Wilkinson. Neutron detection with imaging plates Part I: Image storage and readout. **Nuclear Instruments and Methods in Physics Research A** 424 (1999) : 26-33.

[29]   Nobuo Niimura, Yuuko Karasawa, Inchiro Tanaka, Junji Miyahara, Kenji Takahashi, Hiroki Saito, Satoshi Koizumi, Masanori Hidaka. An imaging plate neutron detector. **Nuclear Instruments and Methods in Physics Research A** 349 (1994) : 521-525.

[30]   FujiFilm. **FUJIFILM imaging plate**. Japan : Fujifilm Holding Corporation, (n.d.). Available from: www.fujifilm.com/ [15th May 2014]

[31]   Fujifilm. FujiFilm Science Lab 2002 General-Purpose Analysis Software Multi Gauge Ver2.0 Operation Manual. Version 3.0. Japan : Fujifilm Holding Corporation, 2002.

[32]   Jeff Prosise. A look inside Bitmap files. **PC Mag** 3 December 1996 : 321-324.

[33]   Ferreira T and Rasband WS. **ImageJ User Guide — IJ 1.46** [Online]. 2012. Available from: imagej.nih.gov/ij/docs/guide/ [3rd October 2014]

[34]   John R. Lamarsh and Anthony J. Baratta. **Introduction to Nuclear Engineering**. Third edition. New Jersey : Prentice Hall, 2001.

[35]   P. Rinard. Neutron interactions with matter. **Passive Nondestructive Assay of Nuclear Materials** (1991) : 357-377.

[36]   Viktor Zerkin. **Evaluated Nuclear Data File (ENDF) Database Version of September 02 2015** [Online]. IAEA, 2015.   Availabe from: https://www-nds.iaea.org/exfor/endf.htm [31st August 2015]

APPENDIX

VITA

Chia Jia Yi was born in Selangor, Malaysia on 4th October, 1990. She graduated from The National University of Malaysia (UKM), Selangor, Malaysia with a Bachelor of Science degree in Nuclear Science in October of 2013. In the same year, she continued her education at Chulalongkorn University, Thailand in pursuit of a Master of Science degree in Nuclear Technology.